iScience

CellPress
OPEN ACCESS

Article

Functional Characterization of Three-Dimensional Cortical Cultures for *In Vitro* Modeling of Brain Networks

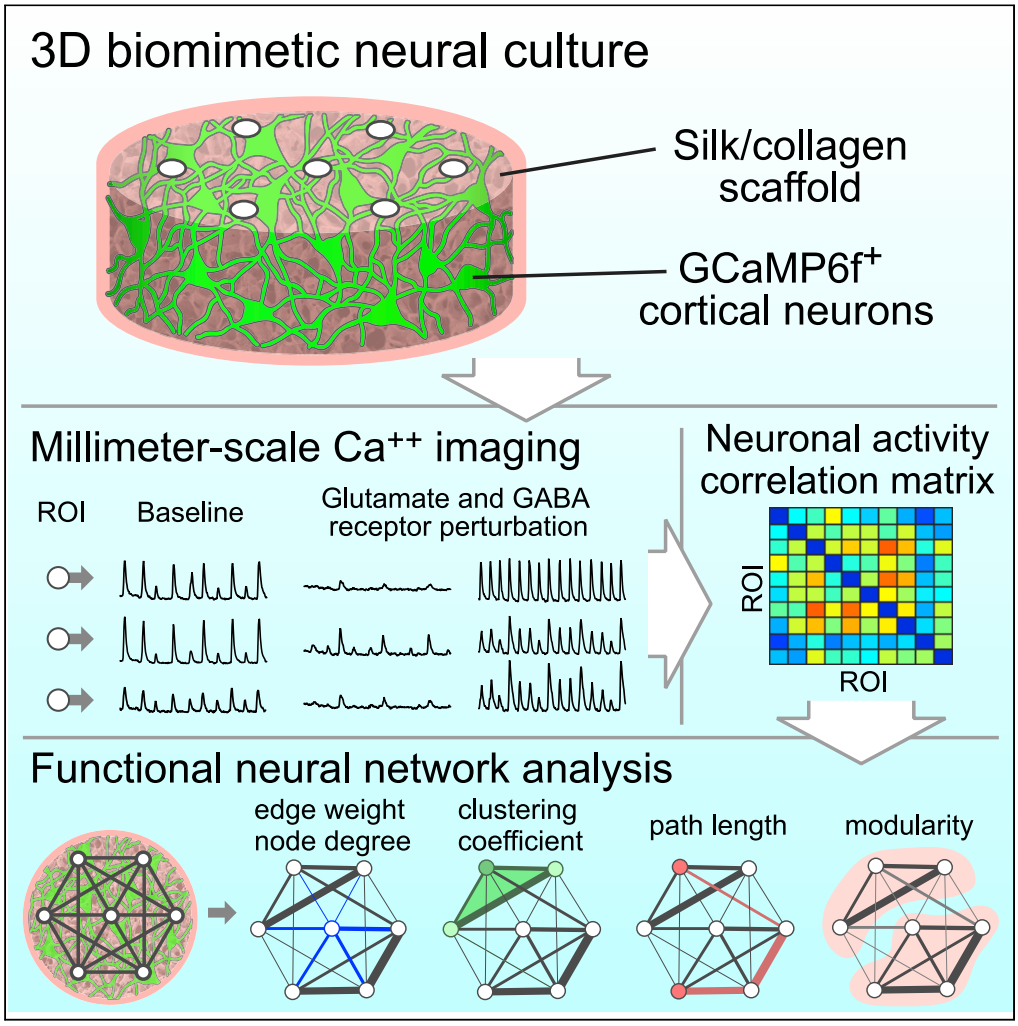

Yu-Ting L. Dingle, Volha Liaudanskaya, Liam T. Finnegan, ..., Irene Georgakoudi, Thomas J.F. Nieland, David L. Kaplan

david.kaplan@tufts.edu

HIGHLIGHTS

3D biomimetic *in vitro* cultures engineered to study functional neural networks

Millimeter-scale network analysis using GCaMP6f expression and widefield microscopy

Connected, unspecialized networks form in the developing 3D neural culture

Network properties change upon pharmacological perturbations of neurotransmission

Dingle et al., iScience *23*, 101434
August 21, 2020
https://doi.org/10.1016/j.isci.2020.101434

iScience

CellPress
OPEN ACCESS

Article

Functional Characterization of Three-Dimensional Cortical Cultures for *In Vitro* Modeling of Brain Networks

Yu-Ting L. Dingle,[1] Volha Liaudanskaya,[1] Liam T. Finnegan,[1] Kyler C. Berlind,[1] Craig Mizzoni,[1] Irene Georgakoudi,[1] Thomas J.F. Nieland,[1] and David L. Kaplan[1,2,*]

SUMMARY

Three-dimensional (3D) *in vitro* cultures recapitulate key features of the brain including morphology, cell-cell and cell-extracellular matrix interactions, gradients of factors, and mechanical properties. However, there remains a need for experimental and computational tools to investigate network functions in these 3D models. To address this need, we present an experimental system based on 3D scaffold-based cortical neuron cultures in which we expressed the genetically encoded calcium indicator GCaMP6f to record neuronal activity at the millimeter-scale. Functional neural network descriptors were computed with graph-theory-based network analysis methods, showing the formation of functional networks at 3 weeks of culture. Changes to the functional network properties upon perturbations to glutamatergic neurotransmission or GABAergic neurotransmission were quantitatively characterized. The results illustrate the applicability of our 3D experimental system for the study of brain network development, function, and disruption in a biomimetic microenvironment.

INTRODUCTION

Three-dimensional (3D) neural cultures recapitulate the cell-cell and cell-extracellular matrix (ECM) interactions of the native brain tissue more accurately than conventional 2D cultures (Zhuang et al., 2018). Because they express *in vivo*-like gene, protein and biomarker expression patterns of development, diseases, and network firing, 3D tissue cultures are useful systems to study brain-like functions at the cellular and tissue level (Lovett et al., 2020). In the brain, adhesion contacts and axonal pathfinding are isotropically distributed in a 3D microenvironment, with neurons synapsing with their immediate neighbors as well as distant neurons in all three dimensions to form extensive neural networks. These interactions are not recapitulated in 2D cultures, where neuronal connections are restricted unnaturally to the x-y plane (Ulloa Severino et al., 2016).

Several 3D culture platforms have been developed to model brain tissues in the laboratory. These platforms generally utilize self-assembly and self-organization principles (e.g., spheroids and organoids) (Birey et al., 2017; Dingle et al., 2015; Lancaster et al., 2013; Quadrato et al., 2017), with or without biomaterial support (e.g., hydrogels or scaffolds) (Frega et al., 2014; Tang-Schomer et al., 2014; Ulloa Severino et al., 2016). One example is our versatile composite scaffold consisting of silk and ECM components for 3D *in vitro* culture. These systems accommodate the long-term growth and function of rodent primary neurons as well as human neurons derived from induced pluripotent stem cells (iPSCs), induced neural stem cells (iNSCs), or other cell types isolated from patient brain or tumor explants (Cairns et al., 2016; Cantley et al., 2018; Lovett et al., 2020; Rouleau et al., 2020; Sood et al., 2016, 2019; Tang-Schomer et al., 2014).

One of the key challenges with using 3D *in vitro* cultures is the functional analysis of the engineered brain-like circuitry. Among the neural network analysis technologies, multi-electrode arrays (MEA) and optical-based approaches such as calcium (Ca^{++}) and voltage imaging provide investigators detailed information on the spatial-temporal aspects of brain network development and function of rodent and human neurons *in vitro* (Badura et al., 2014; Poli et al., 2015; Trujillo et al., 2019). Brain network architecture is a hierarchical entity at multiple spatial scales ranging from connections between synapses to connections between brain regions (Bassett et al., 2018; Betzel and Bassett, 2017). Although MEA offer excellent temporal resolution,

[1]Department of Biomedical Engineering, Tufts University, 200 College Avenue, Medford, MA 02155, USA

[2]Lead Contact

*Correspondence: david.kaplan@tufts.edu

https://doi.org/10.1016/j.isci.2020.101434

cells needs to be in proximity to the electrodes to be detected, and the spatial resolution is physically fixed to the number and spacing of electrodes (typically in the tens to hundreds of μm) (Bourke et al., 2018; Obien et al., 2015; Smith et al., 2015; Tedesco et al., 2018). In contrast to MEA, optical-imaging-based approaches using dyes or genetically encoded reporter constructs have the spatial resolution as high as the microscope equipment allows (typically sub-μm) and have the potential to record contribution of all cells, enabling researchers to conduct analysis at different spatial scales. An optical approach can also be more widely used than MEA due to MEA's requirement of dedicated equipment. Optical analyses of neural networks generally focus on cellular activity patterns at a fraction of 3D space (100–500 μm field width at a single x-y plane) due to the technical limitations of imaging equipment (Bosi et al., 2015; Gu et al., 2016; Huang et al., 2014; Sakaguchi et al., 2019; Ulloa Severino et al., 2016), with few exceptions (Dana et al., 2014; Lu et al., 2020; Palazzolo et al., 2017; Wu et al., 2020). There is a demand for tools to evaluate functional networks at larger, millimeter-scale in 3D cultures.

The objective of the present study was to develop an experimental 3D *in vitro* system that addressed this need through the incorporation of bioengineering principles, genetically encoded calcium indicators (GECIs), widefield microscopy image acquisition, and computational analysis. The output of this experimental system is a set of mathematical parameters describing the functional neural networks that investigators can use to quantitatively compare networks formed under different conditions. Primary mouse cortical neurons were cultured in 3D scaffolds and virally infected with genetic constructs expressing the calcium reporter GCAMP6f (Chen et al., 2013) to monitor activity. Network analysis showed functionally connected neural networks in the 3D cortical cultures. We demonstrated the utility of this experimental system with pharmacological perturbation of glutamatergic excitatory inputs (treatment with D-2-amino-5-phosphonovalerate, AP5; or 2,3-Dioxo-6-nitro-1,2,3,4-tetrahydrobenzo[f]quinoxaline-7-sulfonamide, NBQX) or γ-aminobutyric acid (GABA) inhibitory inputs (treatment with bicuculline or picrotoxin) and presented quantitative outcomes in the network descriptors. Bicuculline and picrotoxin increased neuronal activity, NBQX greatly reduced neuronal activity and impaired the functional network, and AP5 reduced neuronal activity to an even greater degree than NBQX. Interestingly, between the two GABA receptor antagonists, only bicuculline resulted in changes in the functional network properties at the scale we analyzed. Collectively, these data demonstrate the applicability of our 3D *in vitro system* for understanding the links between neurotransmission and network connectivity and for further investigation of the function and disruption of neural networks in a pathophysiological context.

RESULTS

3D *In Vitro* Biomimetic Cortical Culture System to Study Neural Network Structure and Function

To investigate neural network formation in 3D microenvironments, we adapted our previously published *in vitro* composite (silk and collagen) scaffold culture system that mimics the softness of native brain tissue and allows for growth and interaction of neurons and glial cells in three dimensions (Chwalek et al., 2015; Tang-Schomer et al., 2014). Additional elements incorporated into the system in this study were (1) expression of a GECI, GCaMP6f (Chen et al., 2013), as a reporter of neuronal activity, (2) widefield epifluorescence microscopy to record activity at micrometer- and millimeter-scales, and (3) computational tools adapted from published algorithms to investigate functional connectivity of the neural network (Muldoon et al., 2016; Newman, 2006; Onnela et al., 2005; Patel et al., 2015). The scaffolds were fabricated following established protocols, with dimensions optimized for high density cell seeding and for imaging the neural network in one single field of view (scaffold diameter = 3 mm, height = 1.5 mm, volume = 10.6 mm^3 and pore size = 425–500 μm) (Figures 1 and S1). Two million cells were seeded per scaffold (Figure S1). The seeding efficiency was approximately 60%–70%, determined by amount of DNA in the 3D culture relative to a 2 x 10^6 cell pellet with a PicoGreen DNA quantification assay (Figure S2). The cell density in the 3D culture was approximately 1.2—1.3 x 10^6 cells/mm^3.

Development of Neural Networks in the Biomimetic Cortical Culture

Confocal z stack images at 1, 2, and 3 weeks of culture showed that neurons formed extensive 3D structural networks (Figures 2A and 2B, and Video S1). Using a custom MATLAB code to quantify the 3D neurite density ((Liaudanskaya et al., 2020) and detailed in Transparent Methods), we observed an increase in neurite density over the course of development (Figure 2C). To provide further evidence of structural network formation, quantitative real-time PCR (qRT-PCR) was used to analyze the expression of genes known to change during neural development. As anticipated, we observed a downregulation in mRNA expression

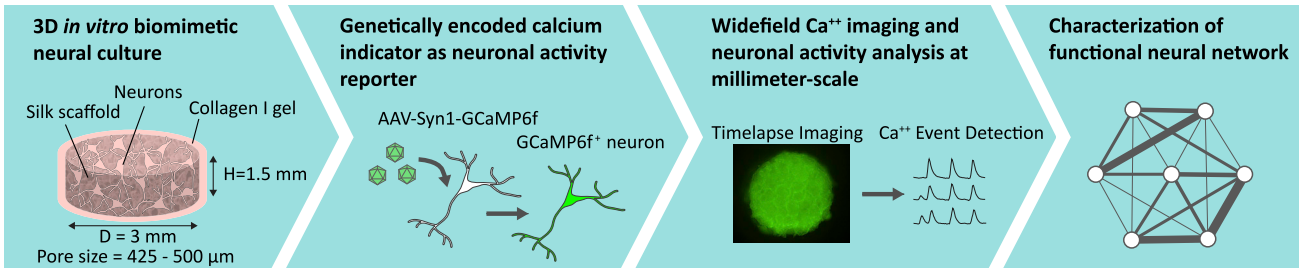

Figure 1. Schematic of the 3D Bioengineered Experimental Platform for Investigating Functional Neural Networks

levels of the neural progenitor marker (*Pax6*) and the immature neuron marker (*Dcx*) (Figure 2D) (Francis et al., 1999; Manuel et al., 2015). We detected a significant upregulation of mRNA encoding proteins with roles in presynaptic vesicle trafficking (*Syn1*), postsynaptic scaffolding (*Shank3*), glutamatergic neurotransmission (*Slc17a7, Gria1, Grin1*), and GABAergic neurotransmission (*GAD2, Gabra1*) (Figure 2D). The increased gene expression of the *Slc3a1* excitatory amino acid transporter together with immunofluorescence imaging of the astrocyte marker glial fibrillary acidic protein (GFAP) indicated the presence of astrocytes in the 3D cultures (Figure 3). Taken together, the data suggest neuronal maturation and synapse formation in the 3D culture model (Ben-Ari, 2001).

3D Cultures Display Spontaneous Neuronal Activities Recorded with a Genetically Encoded Calcium Indicator

For functional analysis of network activity in our 3D biomimetic cortical culture, a GCaMP6f (Chen et al., 2013) genetic construct was expressed in neurons for recording temporal calcium (Ca^{++}) concentration changes, called Ca^{++} transients. The cultures were infected at 1 day *in vitro* (DIV) with adeno-associated virus serotype 1 (AAV1) driving expression in neurons of GCaMP6f under the control of the synapsin 1 promoter (Figure S1). A standard widefield fluorescence microscope with a 4× objective (field size = 4.15× 3.51 mm^2) was used to record the activity patterns from projection of the 3D culture (Figure 4A). Imaging was done for 1-min duration at 5 Hz, the temporal resolution that was sufficient to detect Ca^{++} events in a time-lapse series (Badura et al., 2014).

Neuronal activity was recorded at 2 and 3 weeks of culture, concurrent with the time frame in which rodent neurons grown in conventional 2D culture demonstrate increased activity (Chiappalone et al., 2006). At 2 and 3 weeks of culture, Ca^{++} transients were observed in individual neurons that synchronized within small, local clusters of neurons (size 30–100 µm) as well as larger clusters (>1 mm) (Figure 4A, Video S2). To perform quantitative analysis of the neural networks, the image areas were segmented into equal-size hexagonal regions of interest (ROIs) in a honeycomb configuration that covered the complete projection of the 3D culture sample (Figure 4B). We chose an ROI size of side-to-side distance of 500 µm for long-distance analysis based on previous studies, suggesting cortical neuron axon length *in vitro* (Virlogeux et al., 2018). It should be noted that the ROI size is user-defined, and computational analyses presented below were dependent on this initial ROI determination. Once an ROI mask was applied, fluorescence signal intensity from the projected image in each ROI was averaged to produce a time-series trace (Figure 4C). For each of the ROIs, Ca^{++} event detection was performed with the open-source software FluoroSNNAP (Patel et al., 2015). Spontaneous Ca^{++} events were present at both 2 and 3 weeks of culture in the majority (range 89–100%) of ROIs (Figures 4D, 4E, S3A, and S3B). The frequency of Ca^{++} events increased from 2 to 3 weeks (7.1 ± 0.7 events/min at 2 weeks, 12.9 ± 0.8 events/min at 3 weeks; mean ± SEM) (Figure 4F), correlating with the increased expression of markers of synaptic neurotransmission (Figure 2D). The Ca^{++} transients were abolished after tetrodotoxin (TTX) treatment, reflecting the action-potential-dependent nature of the neuronal activities (Figure 4D).

Pharmacological Perturbations in Excitatory and Inhibitory Neurotransmission Alters Neuronal Activity of 3D Cultures

To validate the responsiveness of our experimental system to network perturbations, a pharmacological strategy was employed to disrupt excitatory or inhibitory synaptic transmissions. The 3D cultures were treated with bicuculline (BIC, a competitive antagonist of inhibitory $GABA_A$ receptors), picrotoxin (PTX,

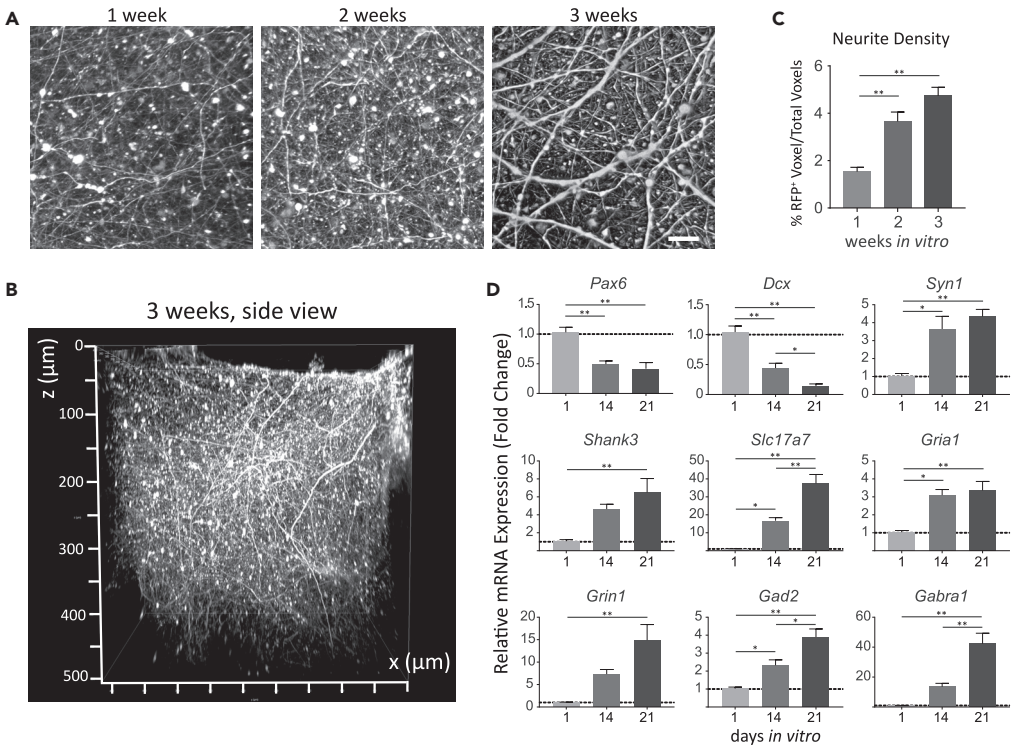

Figure 2. Structural Neural Network Development of the 3D *In Vitro* Biomimetic Cortical Culture

(A) Representative 3D projections of confocal z stack images of RFP-expressing neurons at 1, 2, and 3 weeks. Scale bar, 20 µm.

(B) Representative 3D rendering of side (x-z) view of RFP-expressing neurons at 3 weeks.

(C) Neurite density in the 3D cortical culture (mean ± SEM). n = 6–8 samples from three independent experiments.

(D) mRNA expression over time (mean ± SEM) of proteins associated with neural progenitors (*Pax6*), immature neurons (*Dcx*, doublecortin), presynaptic vesicles (*Syn1*, synapsin 1), postsynaptic scaffolding protein (*Shank3*), glutamatergic transmission (*Slc17a7*, vesicular glutamate transporter 1; *Gria1*, AMPA receptor subunit 1;*Grin1*, NMDA receptor subunit 1), and GABAergic transmission (*GAD2*, glutamate decarboxylase 2; Gabra1, $GABA_A$ receptor subunit α1). Expressions were normalized to housekeeping gene 18s. n = 7–11 samples from three to four independent experiments. For (C) and (D), ANOVA and post-hoc Tukey tests were used for statistical significance among groups. *$p < 0.05$; **$p < 0.001$. See also Video S1. See also Table S2.

a non-competitive antagonist of inhibitory $GABA_A$ and GABAρ receptors), NBQX (a competitive antagonist of excitatory AMPA receptors), or AP5 (a competitive antagonist of excitatory NMDA receptors). Experiments were conducted on 3-week cultures because of their higher baseline activity (Figure 4F).

Spontaneous neuronal activities of each 3D culture sample were recorded and analyzed pre- ("baseline") and post-treatment (Figures 5 and S3, Videos S3, S4, and S5, and Table S1 for detailed numbers and p values). Following treatments with BIC or PTX, Ca^{++} events were present in 100% ROIs. Treatment with NBQX and AP5 significantly reduced the number of ROIs containing Ca^{++} events (post-NBQX, 57 ± 11.8%; post-AP5, 30 ± 10.2%; mean ± SEM). In the AP5-treatment group, 5 of 11 samples (n = 4 experiments) had complete loss of neuronal activity (Figure 5B). Treatment with equivalent concentrations of DMSO, used to dissolve BIC and PTX, had no measurable effects on all the parameters reported in this study (Figure S4).

Both GABA receptor blockers resulted in an increase in Ca^{++} event frequency (BIC group: baseline 10.9 ± 1.1, post-treatment 15.4 ± 0.7; PTX group: baseline 12.3 ± 1.2, post-treatment 17.8 ± 1.1 events/min; mean ± SEM) (Figure 5C). AMPA receptor blocker NBQX reduced the neuronal activity (baseline 10.5 ± 1.0, post-NBQX 2.7 ± 0.9 events/min). Treatment with the NMDA blocker AP5 resulted in greater reduction than NBQX (baseline 11.5 ± 1.6, post-treatment 0.4 ± 0.1 events/min) (Figure 5C). Together, these data show the presence of inhibitory and excitatory transmissions in the 3D tissue cultures and the differential responses of neurons to selective antagonists.

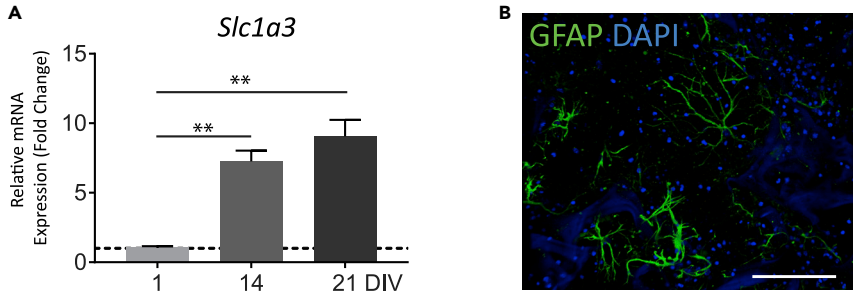

Figure 3. Astrocyte Markers in the 3D Cortical Culture

(A) Relative mRNA expressions at 1, 14, and 21 DIV of *Slc1a3*, excitatory amino acid transporter 1, marker of astrocytes. n = 7–11 samples from three to four independent experiments ANOVA with post-hoc Tukey test was used for statistical significance. **p < 0.001. Scale bar, 100 μm.

(B) Confocal image showing the presence of astrocytes identified by the expression of glial fibrillary acidic protein (GFAP). n = 3 samples from three independent experiments.

Synchronization of neuronal activity in local clusters (5–50 neurons) has been observed *in vivo* during early development, with the level of synchronization changing in a brain-region-dependent manner as neural circuits become more complex (Garaschuk et al., 2000). For *in vitro* studies of networks, a numerical index is used to describe the degree of global synchronization. Here, the global synchronization index was computed by comparing the timing of events in all of the ROIs in each individual 3D culture using FluoroSNNAP software (Patel et al., 2015). An average index of 0.29 ± 0.02 (mean ± SEM) was observed for the 3-week culture baseline conditions. No changes were observed with BIC or PTX treatments (BIC, 0.26 ± 0.04; PTX, 0.29 ± 0.05). In contrast, application of NBQX reduced the global synchronization index (0.14 ± 0.04), suggesting a reduction of global connectivity (Figure 5D). Global synchronization index was not computed for the AP5 group due to lack of neuronal activity.

Functional Neural Network Characterization Using Graph Theory Models: Functional Connectivity, Clustering, Path Length, and Community Structure

A fundamental goal of the field of network neuroscience is to understand brain networks as a complex web of interactions between functional units (Bassett et al., 2018; Lynn and Bassett, 2019). Graph theory is utilized extensively as a mathematical approach to analyze neural network functionality. To demonstrate the applicability of our 3D experimental system for evaluating functional neural networks, we applied previously published graph-theory-based network analyses to evaluate key attributes of the neural networks formed in our 3D cortical cultures at baseline and post-drug treatment conditions (Muldoon et al., 2016; Newman, 2006; Onnela et al., 2005). The basic principle of graph theory is to represent the network as a graph with each user-defined neural unit as a "node" and the connection between two nodes as an "edge" (Figure 6A). In this study, each of the 37 hexagonal ROIs is the equivalent of a node. The functional connectivity (edge) is defined as the statistical similarity of activity patterns of the two nodes, regardless of physical locations or the underlying structural connections.

The functional connectivity between node pairs in the 3D culture was assessed using cross-correlation analysis (Figure 6B). The cross-correlation coefficient of the paired nodes was used as the edge weight, a value to indicate the level of connectivity. These data were then used to compute average clustering coefficient, average path length, community structure, and node degree, which are each described in greater detail below (Figures 6C–6G and see Table S1 for detailed numbers and p values). Average edge weight of all node pairs at baseline and post-BIC, PTX, and NBQX treatments was calculated, but network analysis was not conducted for the AP5 group due to low level of activity. Average edge weight was significantly decreased by the AMPA receptor antagonist NBQX, suggesting a reduction in overall functional connectivity (Figure 6C). Interestingly, between the two GABA receptor antagonists, BIC treatment increased the average edge weight, whereas no significant changes were observed with PTX treatment. These results suggest that BIC, but not PTX, strengthened the overall functional connectivity of the 3D culture.

The average clustering coefficient, a measure of the intensity of functional connectivity among triplets of nodes (detailed in Transparent Methods), was evaluated for our cultures. A network with a high average clustering coefficient is thought to be better at local information integration and more robust to disruption

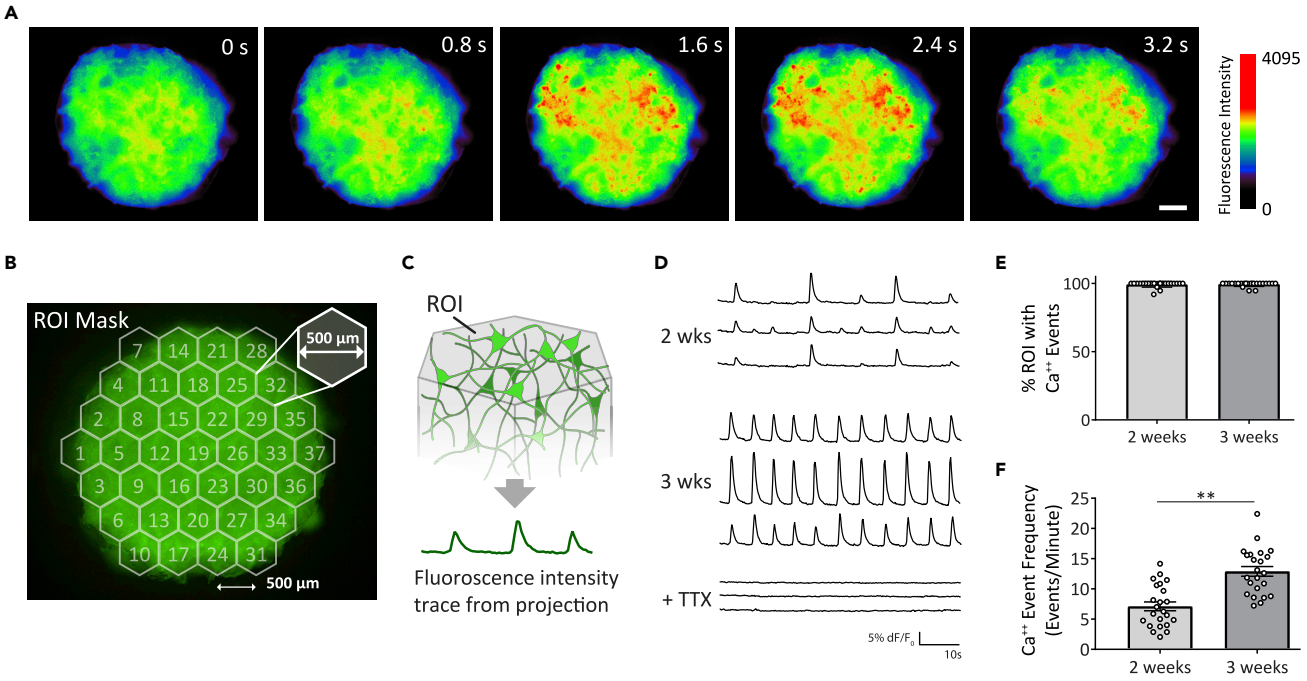

Figure 4. Spontaneous Neuronal Activity in the 3D *In Vitro* Biomimetic Cortical Culture

(A) Representative fluorescence time-lapse image stacks of 3-week-old 3D cultures expressing GCaMP6f. Images are pseudo-colored to highlight Ca^{++} transients. Scale bar, 500 µm.

(B) Mask with 37 hexagonal ROIs (dimensions: area = 0.22 mm^2, side to side and center-to-center distances = 500 µm) is applied to the time-lapse image stack.

(C) Extraction of time-series trace of average fluorescence intensity from the projection of 3D culture in each ROI.

(D) Representative traces of spontaneous Ca^{++} transients from individual ROIs at 2 weeks, 3 weeks, and 3 weeks post-tetrodotoxin (TTX, 40 µM) treatment. Fluorescence changes are normalized to the basal fluorescence intensity (dF/F_0).

(E) Percentage of all ROIs containing Ca^{++} event(s) (mean ± SEM). Each data point represents a unique 3D tissue culture sample.

(F) Ca^{++} event frequency at 2 and 3 weeks (mean ± SEM). Each data point represents average frequency of non-zero event ROIs of a sample. For (E) and (F), n = 23 samples from 3 to 4 matched experiments for 2-week and 3-week samples. An unpaired t test was used for statistical significance. **p < 0.001. See also Figure S5 and Video S2.

(Bullmore and Sporns, 2009; Onnela et al., 2005). In our cultures, an increase in the average clustering coefficient was observed with BIC treatment, whereas no significant changes were observed with PTX treatment. NBQX treatment resulted in a reduction in the average clustering coefficient (Figure 6D). This suggests that acute modulation of GABA and NMDA neurotransmission may alter information integration in our 3D neural networks (Bullmore and Sporns, 2009).

We similarly investigated path length as a descriptor of neural network functionally in our 3D cultures. Inversely proportional to edge weight, the path length is the shortest distance to traverse from one node to another node in the network. In classical network studies, a short average path length suggests that information can be efficiently shared across the network (Muldoon et al., 2016). However, it is important to mention the disagreements with this interpretation in the field (Fornito et al., 2016), and here we use path length as an indication of statistical dependence and not necessarily to characterize information routes. Average path length was calculated from all node pairs and normalized to the number of active nodes (detailed in Transparent Methods). BIC treatment reduced the average path length, whereas PTX had no significant effect (Figure 6E). Because average path length becomes artificially short when only a small portion of nodes remain active (Figure 6B), this descriptor was not calculated for the NMDA-treated cultures.

Many complex networks have community structures in which the network divides naturally into communities, or modules, containing densely interconnected nodes (Newman, 2006). It is hypothesized that community structures play an important role in functional specialization. Examining the community structures can thus provide insights to the specialization of the network (Bullmore and Sporns, 2009). The measurement that describes the strength of segregation of different parts of network into modules is called the

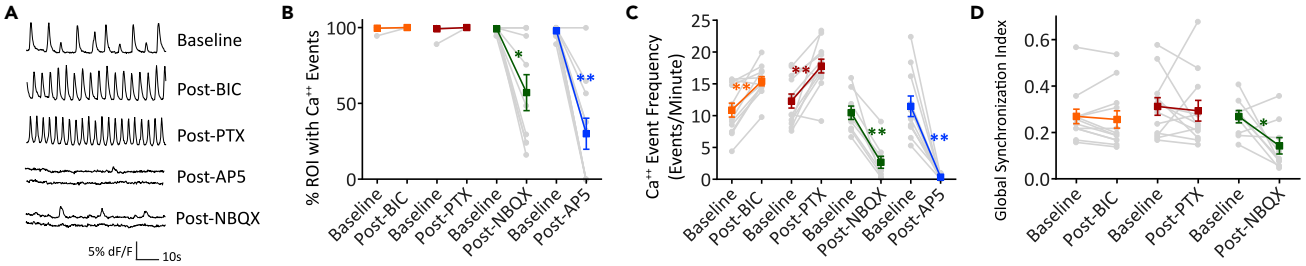

Figure 5. Drug Treatments Induced Neuronal Activity Changes in the 3D Cortical Culture

(A) Representative traces of Ca^{++} transients from individual ROIs in 3-weeks-old 3D cortical culture samples at baseline condition and post-treatments of $GABA_A$ receptor antagonist bicuculline (BIC, 10 μM), $GABA_A$ and GABAρ receptors antagonist picrotoxin (PTX, 50 μM), NMDA receptor antagonist AP5 (50 μM), or AMPA receptor antagonist NBQX (5 μM). Fluorescence changes were normalized to the basal fluorescence intensity (dF/F_0).

(B) Percentage of ROIs in each culture sample containing at least one Ca^{++} event at baseline and post-treatments.

(C) Average Ca^{++} events of all ROIs per sample.

(D) Global synchronization index of Ca^{++} transients across all ROIs in a sample. For (B–D), gray data points and lines show baseline and post-treatment measurements of the same 3D tissue culture samples, and color lines show mean ± SEM. n = 9–12 per group from three to four independent experiments. Paired t tests were used for statistical significance comparing baseline and post-treatment of the same sample. *p < 0.05, **p < 0.001. See also Figure S3, Table S1, and Videos S2, S3, S4, and S5.

modularity (detailed in Transparent Methods). A higher modularity indicates that the network is more strongly divided and the nodes are more interconnected within modules than connected to nodes in other modules. At baseline conditions after 3 weeks of culture, two to three modules formed in the 3D neural network (Figure 6F, top panel) with low modularity (Figure 6F, bottom panel), suggesting a relatively weak community structure. BIC treatment reduced the modularity, whereas PTX had no significant effects. In the NBQX-treated 3D cultures, two different outcomes of community structures were observed. In cultures with fewer than 50% remaining active nodes (3 of 9 cultures), a single module with modularity of 0 was observed, suggesting that the network was deprived of a community structure after losing activity in the majority of nodes. In contrast, in cultures with 75%–100% active nodes, the modularity increased (6 of 9 cultures), suggesting that the network was more strongly divided (Figure 6F, bottom panel). Possible explanations to the variation among samples could be attributed to potential differences in expression level of AMPA receptors and relative level of AMPA receptor- and NMDA receptor-mediated glutamatergic neurotransmissions in each culture at this stage.

Another characteristic of complex networks is the presence of hubs, which facilitate efficient communication by shortening path lengths and bridging modules in a network (Barabási, 2009; Bullmore and Sporns, 2009). Hubs are nodes with a node degree (sum of edge weights touching the node) that greatly exceeds the average. The presence of hub nodes in a network can be inferred by the presence of a non-Gaussian distribution with a long right tail in a frequency distribution plot of node degrees (Schroeter et al., 2015). We computed the node degree for all of the individual nodes and graphed the frequency distribution. The absence of a long right tail in the frequency plots, combined with a normal distribution, indicate the absence of hub nodes under baseline conditions. Neither BIC nor PTX treatments resulted in the emergence of hub nodes. NBQX treatments resulted in a left shift of the node degree distribution because of the observed reduction in functional connectivity of the network, with 49% of the nodes having a node degree of zero (i.e. no remaining functional connectivity) (Figure 6G).

The above analyses were based on ROIs of side-to-side distances of 500 μm. To demonstrate that this model can be used at different spatial scales with other ROI sizes, we repeated the network analyses with smaller ROIs with side-to-side distance of 250 μm on BIC and PTX experiments (Figure S5). Our analyses showed that modifying ROI size from 500 μm to 250 μm changed the raw values of the network descriptors. It did not affect the pre- and post-treatment trends for synchronization, average edge weight, average path length, and modularity. At this scale of analysis, the increase of average clustering coefficient from pre- to post-PTX became statistically significant. This emphasizes that the network analysis is dependent on the initial determination of ROI, which should be chosen based on the question of interest.

In summary, the network analysis indicated that millimeter-sized, functional neural networks developed in the 3D biomimetic cortical cultures. The networks responded to pharmacological perturbations in

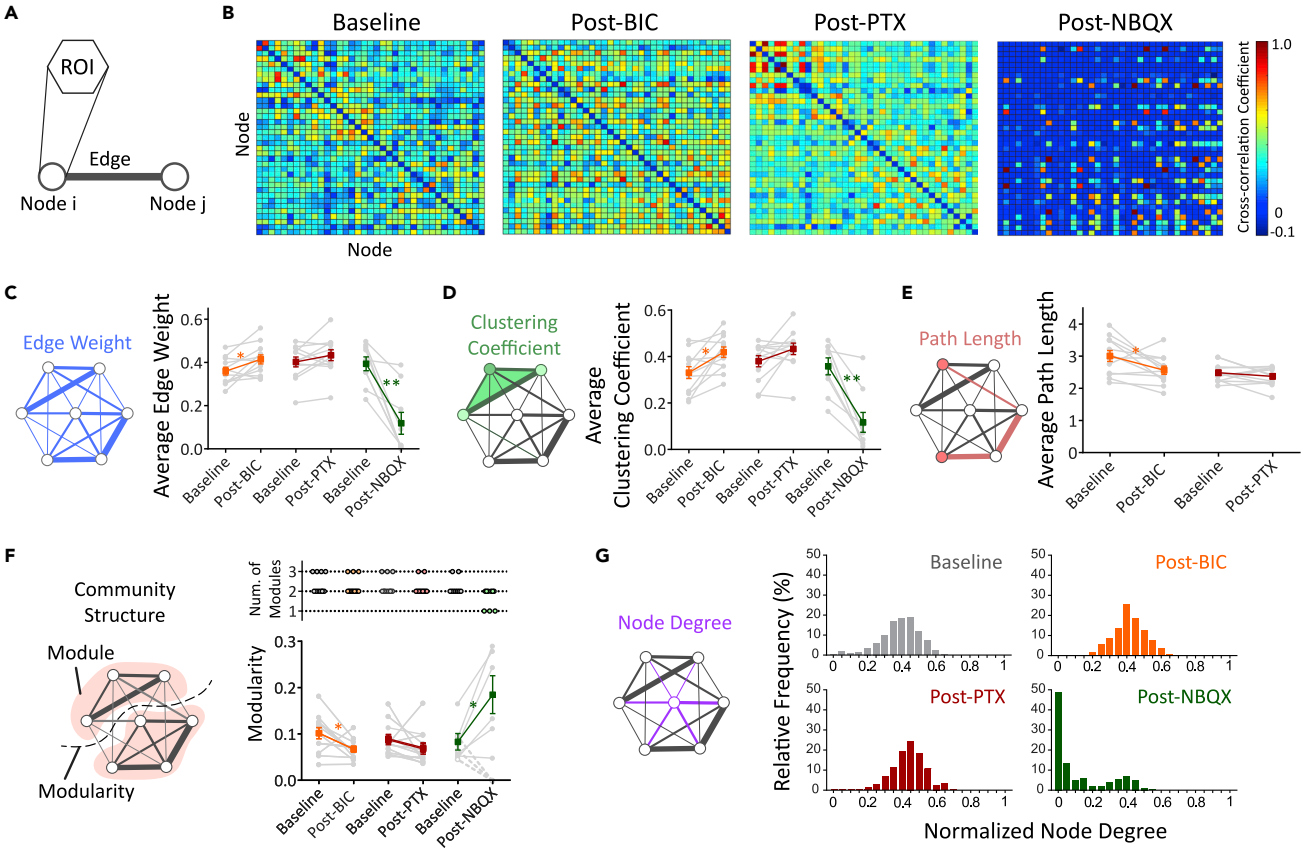

Figure 6. Graph Theory Model-Based Characterizations of Functional Neural Networks in 3D Biomimetic Cortical Cultures

(A) The ROI was designated as a node in the graph-theory-based network analysis.

(B) Representative matrices of cross-correlation coefficients of the 3-week-old 3D cortical culture samples at baseline and post-treatment of bicuculline (BIC; 10 μM), picrotoxin (PTX; 50 μM), or NBQX (5 μM). Self-correlations were removed. The cross-correlation coefficients were then used as edge weight.

(C–F) (C) Average edge weights, (D) average clustering coefficient, (E) average path length, and (F) community structure—number of modules (top) and modularity (bottom) at baseline and post-treatments, as indicated. Post-NBQX samples that lost community structure (1 module and modularity = 0, dotted lines) were excluded from the average modularity calculation.

(G) Frequency distribution of normalized weighted node degree. For (C–F), gray data points and lines represent baseline and post-treatment measurements of individual 3D culture sample. Colored lines show mean ± SEM. (n = 9–12 samples from three to four independent experiments per group). Paired t tests were used for statistical significance comparing baseline and post-treatment of the same sample. *p < 0.05, **p < 0.001. See also Figures S3 and S5, and Table S1.

neurotransmission with measurable changes in the network descriptors. The average edge weight and average clustering coefficient increased with BIC treatment and decreased with NBQX treatment. The average path length decreased with BIC treatment. The networks at 3 weeks of culture had a weak community structure (modularity) and were reduced by BIC treatment. This, combined with the lack of hubs, suggested that unspecialized networks developed in our 3D cultures. These results demonstrate the utility of this 3D culture system for the study of functional neural networks *in vitro*.

DISCUSSION

Functional connection of a neural network is an important field of study for brain function and disorders. Conventional 2D culture with both rodent and human iPSC-derived neurons have been used to investigate neural networks using MEA and optical assays. For example, the correlation patterns of 2D rat cortical neuron cultures over the time frame of 7–35 DIV were evaluated with MEA of 60 electrodes with 200-μm spacing (Chiappalone et al., 2006). The emergency of hub structures in 2D mouse hippocampal neuron cultures were assessed with MEA of 64 electrodes with 200-μm spacing (Schroeter et al., 2015). In the past, network analysis has primarily been done with in-house, customized computer algorithms. FluoroSNNAP software, initially intended for 2D cellular scale analysis, was developed to facilitate the computational

analysis in the field (Patel et al., 2015). Since that time, 3D *in vitro* cultures have become increasingly popular to investigate the development, functions, and disorders of brain networks as they better represent key features of the brain tissue (Lovett et al., 2020; Zhuang et al., 2018). One of the first studies demonstrating network activities in months-old human cortical organoids using MEA (200-μm spacing) and observing changes in synchronized network activities over time was reported (Trujillo et al., 2019). With the increasing popularity of 3D cultures, the field will benefit from tools designed for examining neural networks in greater detail in 3D.

Among the techniques for functional recordings and analysis, optical approaches have the advantages of contact-free, high and flexible spatial resolution, and cell-type-specific targeting (Badura et al., 2014). Here we present an *in vitro* experimental system that allows for interrogation of functional networks that form in a 3D biomimetic microenvironment, with graph-theory-based network analysis that had not been widely utilized by the 3D culture field. The use of a GECI driven by a neuron-specific promotor in combination with observation using widefield microscopy allows for imaging of spatiotemporal patterns in neuronal activity at the millimeter-scale (Figure 1). To describe the functional neural network characteristics and topological properties of our 3D biomimetic cortical culture, we computed several mathematical descriptors (edge weight, clustering coefficient, path length, number of modules, modularity, and node degree). Ca^{++} imaging has been widely used in tissues, both *in vivo* and *ex vivo*, and in other forms of 3D cultures, including organoids. With user-optimized ROI size and Ca^{++} event detection parameters according to the culture's neuronal activities, our network analysis methods can be readily adapted to a wide range of other culture models. We compiled MATLAB algorithms into a user-friendly code and made this available to researchers (https://github.com/yutingdingle/network-analysis) so that it can be applied to other *in vitro* culture models. Additional network descriptors (e.g., shortcuts, core-periphery) (Lynn and Bassett, 2019) can potentially be quantified by plugging in other available open source codes and software (Hassan et al., 2015; Rubinov and Sporns, 2010).

In our 3D experimental system, dense structural networks and spontaneous neuronal activities were detected within 2 weeks of culture. In the neonatal rodent brain, AMPA receptors are initially "silent," and glutamatergic synaptic transmission is purely driven by NMDA receptors. In contrast, activation of AMPA receptor is required for the opening of NMDA receptors in the adult brain (Ben-Ari et al., 1997). At 3 weeks of our 3D culture, a large portion of NMDA receptor activity (blocked by AP5) was independent of AMPA receptors (blocked by NBQX). NMDA receptors were also observed to drive a higher percentage of excitatory activities than AMPA receptors. The glutamatergic neurotransmission of the 3D cultures thus appears to fall within the developmental stage of immature brains at the postnatal stage. In addition, we noticed variations among the 3D cultures' susceptibility to NMDA and AMPA receptors blockers, with one hypothesis being that differences in the expression levels of AMPA and NMDA receptors and the functionality of AMPA receptors among individual 3D samples during neural network formation is the underlying basis for this observation.

Functional networks were established by 3 weeks in the 3D cortical culture. The lack of hubs and weak community structures observed in the networks at this time point can be interpreted as an indication of an unspecialized network (Bullmore and Sporns, 2009; Lynn and Bassett, 2019; Schroeter et al., 2015). It is plausible that our 3D mouse cortical network may develop more specialized features with extended culture time and/or after application of external stimuli in the form of optogenetic actuators (such as channelrhodopsins) and/or biochemical stimuli, such as brain-derived neurotrophic factor (BDNF) (Afshar Saber et al., 2018; Mishchenko et al., 2019).

A functional, balanced neural network relies on the highly regulated integration of the flow of information from both excitatory and inhibitory inputs. We demonstrated that this experimental system can model disruptions in excitatory and inhibitory neurotransmissions and network dysfunctions. Blocking excitatory AMPA receptors with NBQX reduced neuronal activity and disrupted the functional neural network with reductions in edge weight, clustering coefficient, and community structure. Blocking inhibitory GABA receptors with antagonists BIC and PTX increased neuronal activity (indicated by the increase of Ca^{++} event frequency). Interestingly, only BIC treatment resulted in significant changes to functional network descriptors such as increased average edge weight, increased average clustering coefficient, decreased average path length, and decreased modularity, at our chosen spatial scale of analysis. In-depth examination of GABA receptor subtype expressions and distributions are needed to further address the mechanistic differences

in network responses. However, possible explanations for these discrepancies include the differences in targets and mechanisms-of-action of BIC and PTX (i.e., competitive $GABA_A$ receptor antagonist versus non-competitive, allosteric antagonist of both $GABA_A$ and GABAρ, respectively). Considering that the brain undergoes critical changes of GABA, NMDA, and AMPA receptor isoforms and functions during development *in vivo*, our 3D culture system may provide a useful *in vitro* tool to further examine how changes in receptor expressions shape functional network formation.

The inherent flexibility of our bioengineering approach allows for expression of other genetically encoded constructs to induce (e.g., optogenetic tools) and record cell and network activities (e.g., voltage sensitive and glutamate reporters) (Afshar Saber et al., 2018; Mutoh et al., 2012). Furthermore, high-speed recording of large 3D networks with cellular resolution may be possible using light-sheet confocal microscopy. Another distinct advantage of our scaffold-based bioengineering approach is the possibility of tailoring the organization, compartmentalization, and mechanical properties of the 3D culture to better match that of the native brain. For instance, specific cell-types (e.g., astrocytes, microglia, oligodendrocytes, or other neural subtypes), as well as their ratio and density, can be customized in our 3D cultures to mimic white and gray matter structure (Tang-Schomer et al., 2014), to create specific cellular interactions (e.g., neural circuits), and/or to study interactions between cells and varied ECM compositions (Sood et al., 2016). We hypothesize that systematic testing of these input parameters will advance the bioengineering of 3D *in vitro* biomimetic models to more closely mimic the network density and functional connectivity of the brain.

The 3D *in vitro* biomimetic culture approach would be particularly useful to study the many human brain disorders that are thought to be caused by dysfunction in the structure and function of synapses and neural circuits (Busche and Konnerth, 2016; Cantley et al., 2018; Centeno et al., 2018; Watanabe and Rees, 2016). For instance, we recently observed Alzheimer-disease-related changes in our long-lived 3D human, iPSC-derived neuron-astrocyte co-cultures grown in silk scaffolds (Rouleau et al., 2020). This suggests that our 3D experimental system has utility as a model for long-term studies to the onset and progression of neurodegenerative and neurodevelopmental disorders. In summary, our interdisciplinary experimental system consisting of a 3D *in vitro* biomimetic neural culture, genetically encoded neuronal activity reporter, widefield imaging acquisition, and graph-theory-based network analysis adds a valuable new tool for investigating development, function, and disorders of brain networks.

Limitations of the Study

The brain is organized into circuits in which diverse types of neurons connect over multiple spatial scales in a 3D space, ranging from synaptic connections to connections between brain regions. In the present study, we utilized readily accessible standard widefield microscopy to conduct millimeter-scale analysis of 3D mouse cortical cultures at the expense of resolution and the analysis in the third dimension. In comparison to 2D cultures, where all the information flow within the field of view is captured, our platform integrated the 3D information onto a projection and information flow in the Z-dimension is lost. In order to capture Ca^{++} transients with high spatial resolution and at multilayers at the necessary speed for single-cell and/or 3D analysis, advanced microscopy technologies such as high-speed light-sheet confocal or two-photon microscopy will be crucial. These functional neural networks change dynamically during one's lifespan. Our functional network characterization was conducted in mouse cultures at a 3-week time point. Future studies could incorporate human iPSC-derived cultures to investigate time-dependent development of neural network functions and the biology of brain disease.

Resource Availability

Lead Contact

David Kaplan, Ph.D., david.kaplan@tufts.edu.

Materials Availability

This study did not generate new unique reagents.

Data and Code Availability

The code generated during this study is available at https://github.com/yutingdingle/network-analysis.

METHODS

All methods can be found in the accompanying Transparent Methods supplemental file.

SUPPLEMENTAL INFORMATION

Supplemental Information can be found online at https://doi.org/10.1016/j.isci.2020.101434.

ACKNOWLEDGMENTS

This work was supported by National Institutes of Health (NIH) research grants R01NS092847 and P41EB027062 to DLK, and NIH S10 OD021624 and National Science Foundation MRI 1531683 research infrastructure grants to Tufts University. The authors would like to thank Mattia Bonzanni, Ph.D., for guidance on network analysis models, constructing the computational framework and writing the MATLAB code for network analysis, and assistance with interpreting results; Martin Hunter for assistance with confocal microscopy; Nilay Vora for writing the preliminary Ca^{++} peak detection MATLAB code; Patrick Dingle for writing the MATLAB and Python codes for batch processing data; Allison Sweeney for data processing for neurite density imaging analysis; and Michael Lovett, Ph.D., for reading the manuscript.

AUTHOR CONTRIBUTIONS

Conceptualization, Y.L.D., T.J.F.N., and D.L.K.; Methodology, Y.L.D., V.L., and T.J.F.N.; Software, Y.L.D, V.L., C.M., and I.G.; Formal Analysis, Y.L.D., V.L., and L.T.F.; Investigation, Y.L.D., V.L., L.T.F., and K.C.B.; Writing—Original Draft, Y.L.D. and T.J.F.N.; Writing—Review & Editing, I.G., T.J.F.N., and D.L.K; Visualization, Y.L.D.; Supervision, T.J.F.N. and D.L.K.; Funding Acquisition, D.L.K.

DECLARATION OF INTERESTS

The authors declare no competing interests.

Received: April 9, 2020
Revised: June 27, 2020
Accepted: August 3, 2020
Published: August 21, 2020

REFERENCES

Afshar Saber, W., Gasparoli, F.M., Dirks, M.G., Gunn-Moore, F.J., and Antkowiak, M. (2018). All-optical assay to study biological neural networks. Front. Neurosci. *12*, 451.

Badura, A., Sun, X.R., Giovannucci, A., Lynch, L.A., and Wang, S.S. (2014). Fast calcium sensor proteins for monitoring neural activity. Neurophotonics *1*, 025008.

Barabási, A.-L. (2009). Scale-free networks: a decade and beyond. Science *325*, 412.

Bassett, D.S., Zurn, P., and Gold, J.I. (2018). On the nature and use of models in network neuroscience. Nat. Rev. Neurosci. *19*, 566–578.

Ben-Ari, Y. (2001). Developing networks play a similar melody. Trends Neurosci. *24*, 353–360.

Ben-Ari, Y., Khazipov, R., Leinekugel, X., Caillard, O., and Gaiarsa, J.-L. (1997). $GABA_A$, NMDA and AMPA receptors: a developmentally regulated 'ménage à trois. Trends Neurosci. *20*, 523–529.

Betzel, R.F., and Bassett, D.S. (2017). Multi-scale brain networks. Neuroimage *160*, 73–83.

Birey, F., Andersen, J., Makinson, C.D., Islam, S., Wei, W., Huber, N., Fan, H.C., Metzler, K.R.C., Panagiotakos, G., Thom, N., et al. (2017). Assembly of functionally integrated human forebrain spheroids. Nature *545*, 54–59.

Bosi, S., Rauti, R., Laishram, J., Turco, A., Lonardoni, D., Nieus, T., Prato, M., Scaini, D., and Ballerini, L. (2015). From 2D to 3D: novel nanostructured scaffolds to investigate signalling in reconstructed neuronal networks. Sci. Rep. *5*, 9562.

Bourke, J.L., Quigley, A.F., Duchi, S., O'Connell, C.D., Crook, J.M., Wallace, G.G., Cook, M.J., and Kapsa, R.M.I. (2018). Three-dimensional neural cultures produce networks that mimic native brain activity. J. Tissue Eng. Regen. Med. *12*, 490–493.

Bullmore, E., and Sporns, O. (2009). Complex brain networks: graph theoretical analysis of structural and functional systems. Nat. Rev. Neurosci. *10*, 186–198.

Busche, M.A., and Konnerth, A. (2016). Impairments of neural circuit function in Alzheimer's disease. Philos. Trans. R. Soc. Lond. B Biol. Sci. *371*, 20150429.

Cairns, D.M., Chwalek, K., Moore, Y.E., Kelley, M.R., Abbott, R.D., Moss, S., and Kaplan, D.L. (2016). Expandable and rapidly differentiating human induced neural stem cell lines for multiple tissue engineering applications. Stem Cell Reports *7*, 557–570.

Cantley, W.L., Du, C., Lomoio, S., DePalma, T., Peirent, E., Kleinknecht, D., Hunter, M., Tang-Schomer, M.D., Tesco, G., and Kaplan, D.L. (2018). Functional and sustainable 3D human neural network models from pluripotent stem cells. ACS Biomater. Sci. Eng. *4*, 4278–4288.

Centeno, E.G.Z., Cimarosti, H., and Bithell, A. (2018). 2D versus 3D human induced pluripotent stem cell-derived cultures for neurodegenerative disease modelling. Mol. Neurodegener *13*, 27.

Chen, T.W., Wardill, T.J., Sun, Y., Pulver, S.R., Renninger, S.L., Baohan, A., Schreiter, E.R., Kerr, R.A., Orger, M.B., Jayaraman, V., et al. (2013). Ultrasensitive fluorescent proteins for imaging neuronal activity. Nature *499*, 295–300.

Chiappalone, M., Bove, M., Vato, A., Tedesco, M., and Martinoia, S. (2006). Dissociated cortical networks show spontaneously correlated activity patterns during in vitro development. Brain Res. *1093*, 41–53.

Chwalek, K., Tang-Schomer, M.D., Omenetto, F.G., and Kaplan, D.L. (2015). In vitro bioengineered model of cortical brain tissue. Nat. Protoc. *10*, 1362–1373.

Dana, H., Marom, A., Paluch, S., Dvorkin, R., Brosh, I., and Shoham, S. (2014). Hybrid multiphoton volumetric functional imaging of large-scale bioengineered neuronal networks. Nat. Commun. *5*, 3997.

Dingle, Y.T., Boutin, M.E., Chirila, A.M., Livi, L.L., Labriola, N.R., Jakubek, L.M., Morgan, J.R., Darling, E.M., Kauer, J.A., and Hoffman-Kim, D. (2015). Three-dimensional neural spheroid culture: an in vitro model for cortical studies. Tissue Eng. Part C Methods *21*, 1274–1283.

Fornito, A., Zalesky, A., and Bullmore, E. (2016). Fundamentals of Brain Network Analysis (Academic Press).

Francis, F., Koulakoff, A., Boucher, D., Chafey, P., Schaar, B., Vinet, M.-C., Friocourt, G., McDonnell, N., Reiner, O., Kahn, A., et al. (1999). Doublecortin is a developmentally regulated, microtubule-associated protein expressed in migrating and differentiating neurons. Neuron *23*, 247–256.

Frega, M., Tedesco, M., Massobrio, P., Pesce, M., and Martinoia, S. (2014). Network dynamics of 3D engineered neuronal cultures: a new experimental model for in-vitro electrophysiology. Sci. Rep. *4*, 5489.

Garaschuk, O., Linn, J., Eilers, J., and Konnerth, A. (2000). Large-scale oscillatory calcium waves in the immature cortex. Nat. Neurosci. *3*, 452–459.

Gu, Q., Tomaskovic-Crook, E., Lozano, R., Chen, Y., Kapsa, R.M., Zhou, Q., Wallace, G.G., and Crook, J.M. (2016). Functional 3D neural mini-tissues from printed Gel-based bioink and human neural stem cells. Adv. Healthc. Mater. *5*, 1429–1438.

Hassan, M., Shamas, M., Khalil, M., El Falou, W., and Wendling, F. (2015). EEGNET: an open source tool for analyzing and visualizing M/EEG connectome. PLoS One *10*, e0138297.

Huang, Z., Sun, Y., Liu, W., Zhang, W., Zheng, W., and Jiang, X. (2014). Assembly of functional three-dimensional neuronal networks on a microchip. Small *10*, 2530–2536.

Lancaster, M.A., Renner, M., Martin, C.A., Wenzel, D., Bicknell, L.S., Hurles, M.E., Homfray, T., Penninger, J.M., Jackson, A.P., and Knoblich, J.A. (2013). Cerebral organoids model human brain development and microcephaly. Nature *501*, 373–379.

Liaudanskaya, V., Chung, J.Y., Mizzoni, C., Rouleau, N., Berk, A.N., Wu, L., Turner, J.A., Georgakoudi, I., Whalen, M.J., Nieland, T.J.F., et al. (2020). Modeling controlled cortical impact injury in 3D brain-like tissue cultures. Adv. Healthc. Mater. *9*, 2000122.

Lovett, M.L., Nieland, T.J.F., Dingle, Y.-T.L., and Kaplan, D.L. (2020). Innovations in 3-dimensional tissue models of human brain physiology and diseases. Adv. Funct. Mater. 1909146.

Lu, R., Liang, Y., Meng, G., Zhou, P., Svoboda, K., Paninski, L., and Ji, N. (2020). Rapid mesoscale volumetric imaging of neural activity with synaptic resolution. Nat. Methods *17*, 291–294.

Lynn, C.W., and Bassett, D.S. (2019). The physics of brain network structure, function and control. Nat. Rev. Phys. *1*, 318–332.

Manuel, M.N., Mi, D., Mason, J.O., and Price, D.J. (2015). Regulation of cerebral cortical neurogenesis by the Pax6 transcription factor. Front. Cell. Neurosci. *9*, 70.

Mishchenko, T.A., Mitroshina, E.V., Usenko, A.V., Voronova, N.V., Astrakhanova, T.A., Shirokova, O.M., Kastalskiy, I.A., and Vedunova, M.V. (2019). Features of neural network formation and their functions in primary hippocampal cultures in the context of chronic TrkB receptor system influence. Front. Physiol. *9*, 1925.

Muldoon, S.F., Bridgeford, E.W., and Bassett, D.S. (2016). Small-world propensity and weighted brain networks. Sci. Rep. *6*, 22057.

Mutoh, H., Akemann, W., and Knopfel, T. (2012). Genetically engineered fluorescent voltage reporters. ACS Chem. Neurosci. *3*, 585–592.

Newman, M.E. (2006). Modularity and community structure in networks. Proc. Natl. Acad. Sci. U S A *103*, 8577–8582.

Obien, M.E.J., Deligkaris, K., Bullmann, T., Bakkum, D.J., and Frey, U. (2015). Revealing neuronal function through microelectrode array recordings. Front. Neurosci. *8*, 423.

Onnela, J.P., Saramaki, J., Kertesz, J., and Kaski, K. (2005). Intensity and coherence of motifs in weighted complex networks. Phys. Rev. E Stat. Nonlin. Soft Matter Phys. *71*, 065103.

Palazzolo, G., Moroni, M., Soloperto, A., Aletti, G., Naldi, G., Vassalli, M., Nieus, T., and Difato, F. (2017). Fast wide-volume functional imaging of engineered in vitro brain tissues. Sci. Rep. *7*, 8499.

Patel, T.P., Man, K., Firestein, B.L., and Meaney, D.F. (2015). Automated quantification of neuronal networks and single-cell calcium dynamics using calcium imaging. J. Neurosci. Methods *243*, 26–38.

Poli, D., Pastore, V.P., and Massobrio, P. (2015). Functional connectivity in in vitro neuronal assemblies. Front. Neural Circuits *9*, 57.

Quadrato, G., Nguyen, T., Macosko, E.Z., Sherwood, J.L., Min Yang, S., Berger, D.R., Maria, N., Scholvin, J., Goldman, M., Kinney, J.P., et al. (2017). Cell diversity and network dynamics in photosensitive human brain organoids. Nature *545*, 48–53.

Rouleau, N., Cantley, W.L., Liaudanskaya, V., Berk, A., Du, C., Rusk, W., Peirent, E., Koester, C., Nieland, T.J.F., and Kaplan, D.L. (2020). A long-living bioengineered neural tissue platform to study neurodegeneration. Macromol. Biosci. *20*, e2000004.

Rubinov, M., and Sporns, O. (2010). Complex network measures of brain connectivity: uses and interpretations. Neuroimage *52*, 1059–1069.

Sakaguchi, H., Ozaki, Y., Ashida, T., Matsubara, T., Oishi, N., Kihara, S., and Takahashi, J. (2019). Self-organized synchronous calcium transients in a cultured human neural network derived from cerebral organoids. Stem Cell Reports *13*, 458–473.

Schroeter, M.S., Charlesworth, P., Kitzbichler, M.G., Paulsen, O., and Bullmore, E.T. (2015). Emergence of rich-club topology and coordinated dynamics in development of hippocampal functional networks in vitro. J. Neurosci. *35*, 5459–5470.

Smith, I., Haag, M., Ugbode, C., Tams, D., Rattray, M., Przyborski, S., Bithell, A., and Whalley, B.J. (2015). Neuronal-glial populations form functional networks in a biocompatible 3D scaffold. Neurosci. Lett. *609*, 198–202.

Sood, D., Chwalek, K., Stuntz, E., Pouli, D., Du, C., Tang-Schomer, M., Georgakoudi, I., Black, L.D., 3rd, and Kaplan, D.L. (2016). Fetal brain extracellular matrix boosts neuronal network formation in 3D bioengineered model of cortical brain tissue. ACS Biomater. Sci. Eng. *2*, 131–140.

Sood, D., Tang-Schomer, M., Pouli, D., Mizzoni, C., Raia, N., Tai, A., Arkun, K., Wu, J., Black, L.D., 3rd, Scheffler, B., et al. (2019). 3D extracellular matrix microenvironment in bioengineered tissue models of primary pediatric and adult brain tumors. Nat. Commun. *10*, 4529.

Tang-Schomer, M.D., White, J.D., Tien, L.W., Schmitt, L.I., Valentin, T.M., Graziano, D.J., Hopkins, A.M., Omenetto, F.G., Haydon, P.G., and Kaplan, D.L. (2014). Bioengineered functional brain-like cortical tissue. Proc. Natl. Acad. Sci. U S A *111*, 13811–13816.

Tedesco, M.T., Di Lisa, D., Massobrio, P., Colistra, N., Pesce, M., Catelani, T., Dellacasa, E., Raiteri, R., Martinoia, S., and Pastorino, L. (2018). Soft chitosan microbeads scaffold for 3D functional neuronal networks. Biomaterials *156*, 159–171.

Trujillo, C.A., Gao, R., Negraes, P.D., Gu, J., Buchanan, J., Preissl, S., Wang, A., Wu, W., Haddad, G.G., Chaim, I.A., et al. (2019). Complex oscillatory waves emerging from cortical organoids model early human brain network development. Cell Stem Cell *25*, 558–569 e557.

Ulloa Severino, F.P., Ban, J., Song, Q., Tang, M., Bianconi, G., Cheng, G., and Torre, V. (2016). The role of dimensionality in neuronal network dynamics. Sci. Rep. *6*, 29640.

Virlogeux, A., Moutaux, E., Christaller, W., Genoux, A., Bruyere, J., Fino, E., Charlot, B., Cazorla, M., and Saudou, F. (2018). Reconstituting corticostriatal network on-a-chip reveals the contribution of the presynaptic compartment to Huntington's disease. Cell Rep *22*, 110–122.

Watanabe, T., and Rees, G. (2016). Anatomical imbalance between cortical networks in autism. Sci. Rep. *6*, 31114.

Wu, J., Liang, Y., Chen, S., Hsu, C.-L., Chavarha, M., Evans, S.W., Shi, D., Lin, M.Z., Tsia, K.K., and Ji, N. (2020). Kilohertz two-photon fluorescence microscopy imaging of neural activity in vivo. Nat. Methods *17*, 287–290.

Zhuang, P., Sun, A.X., An, J., Chua, C.K., and Chew, S.Y. (2018). 3D neural tissue models: from spheroids to bioprinting. Biomaterials *154*, 113–133.

iScience, Volume *23*

Supplemental Information

Functional Characterization of Three-Dimensional Cortical Cultures for *In Vitro* Modeling of Brain Networks

Yu-Ting L. Dingle, Volha Liaudanskaya, Liam T. Finnegan, Kyler C. Berlind, Craig Mizzoni, Irene Georgakoudi, Thomas J.F. Nieland, and David L. Kaplan

Supplementary Information

Transparent Methods

Silk fibroin scaffold fabrication

A 6 % (w/v) silk fibroin solution was used to prepare silk fibroin porous sponge scaffolds (pore size 425 – 500 µm) as previously described (Chwalek et al., 2015; Tang-Schomer et al., 2014). Briefly, *Bombyx mori* cocoons (Tajima Shoji Co., Ltd, Japan) were cut into small pieces and boiled in 0.02 M sodium carbonate (MilliporeSigma #57795) solution for 30 min to remove sericin. Dry silk fibroin fibers were dissolved in 9.3 M lithium bromide (LiBr, MilliporeSigma #213225) solution at 60°C for 4 hrs. The solution was dialyzed against water in dialysis tubing (Fisher #21-152-9, molecular weight cutoff 3,500 Da) for 2 days with six 4 L water changes over 48 hours to remove LiBr. Undissolved material was removed by centrifuging twice at 12,700 rcf at 4°C for 30 min followed by passing through a cell strainer with 100-µm pore size (Corning #431752). The resulting silk fibroin solution was adjusted to 6 % (w/v) with water. Sodium chloride (NaCl) was sieved to 425 – 500 µm particle size. Thirty mL of 6% silk fibroin solution was poured into a 10-cm petri dish, and 60 g of NaCl was poured evenly into the solution. The silk fibroin was left at room temperature for 2 days and incubated at 60°C for 1 hr to allow the silk fibroin to form insoluble β-sheet crystalline structure. The resulting material was freed from the petri dish and rinsed in 4 L water for 2 days with 6 water exchanges to remove the NaCl particles and leave behind the resulting pores. Silk scaffolds for the biomimetic cortical cultures were cut into 3-mm diameter and 1.5-mm height cylinders using a biopsy punch (Integra #12-460-406) and a razor blade.

3D cortical cultures and AAV infections

All 3D cortical cultures were maintained, unless otherwise noted, in Neuro Medium: Neurobasal Medium (ThermoFisher #21103) or Neurobasal Medium minus phenol red (ThermoFisher #12348) supplemented with 2% B27 (ThermoFisher #17504), 1% Antibiotic-Antimycotic (ThermoFisher #15240), and 2 mM GlutaMax (ThermoFisher #35050).

Scaffolds were placed in water and sterilized by autoclaving. Prior to cell seeding, scaffolds were coated overnight with poly-D-lysine (PDL; 0.1 mg/mL in water, MilliporeSigma #P6407) and laminin (LN; 10 µg/mL, MilliporeSigma #MFCD00081739). Typically, in a 12-well we coat 20-30 sponges in 2 mL coating solution. On the day of cell seeding, the scaffolds were washed twice with PBS (10-min incubation), then incubated at least for one hour with Neuro Medium and at least for one hour in Neuro Medium containing 5% (v/v) fetal bovine serum (FBS). Excess medium was aspirated immediately before cell seeding.

Brain cortices were harvested from E16 C57BL/6 mouse embryos (Charles River Laboratories) and digested with 0.25% Trypsin (Thermo Fisher #325200) and 0.3 mg/mL DNase (MilliporeSigma #10104159001). All animal procedures were approved by Tufts University Institutional Animal Care and Use Committee (IACUC, Protocol #M2018-06). Neurons were resuspended in Neuro Medium containing 5% FBS at the density of $2x10^6$ cells per 5 µL. PDL-LN-coated scaffolds aspirated to dry and transferred to a 96-well plate (one scaffold per well). A cell suspension of 5 µL was pipetted directly onto the scaffold, and the seeded scaffolds were incubated in 37˚C for 30 min to allow for cell adhesion, followed by addition of 200 µL Neuro Medium + 5% FBS. The day of cell seeding was referred as 0 days-in-vitro (DIV). The next day (1 DIV), cultures were transferred to 500 µL of medium in 48-well plates. For neurite density image analysis, 3D cultures were infected on 1 DIV with AAV-hSyn1-TurboRFP (pENN.AAV.hSyn.TurboRFP.WPRE.RBG, Addgene #105552-AAV1, titer 2.7 x 10^{13} GC/mL, a gift from Dr. James M. Wilson, unpublished) diluted in Neuro Medium at 1:1000. 3D cultures for DNA quantification, RNA analysis, and immunostaining were transferred to fresh 500 µL Neuro Medium without AAV. For Ca^{++} imaging experiments, 3D cultures were infected with AAV-hSyn1-GCaMP6f (AAV-hSyn1-GCaMP6f-P2A-nls-dTomato, Addgene, #51085-AAV1, titer 2 x 10^{13} GC/mL, a gift from Dr. Jonathan Ting, unpublished) diluted in Neuro Medium at 1:1000. The 3D cultures where then incubated overnight at 37˚C.

On 2 DIV, 3D cultures were transferred to 96-well plates, and 10 µL of 3 mg/mL collagen type I solution (Corning #354236) was pipetted onto each scaffold followed by incubation at 37˚C for 30 min to allow for collagen gelation. Each 3D culture was then transferred to a 24-well containing 2 mL Neuro Medium. For cultures intended for Ca^{++} imaging (AAV-hSyn1-GCaMP6f infected), glass-bottom plates (Cellvis #P24-1.5P) and phenol red-free Neuro Medium were used. Half-media changes were carried out every 3-4 days.

Assessment of 3D neurite density

3D cultures infected with AAV-hSyn1-TurboRFP were chemically fixed on at 1, 2, and 3 wk with 4% paraformaldehyde/4% sucrose in PBS for 1 hr. After three PBS washes (30-min each), the 3D cultures were imaged with a Leica SP8 confocal microscope with a 40X objective (Leica HC PL APO 40x/1.10 W CORR CS2), x,y,z-dimensions= 291 x 291 x 210 µm, 0.42 µm per z-step) with excitation laser of 552 µm. 3D movie (Movie S1) was rendered with maximum projections in LAS X software (Leica). Z-stack images were analyzed using a custom MATLAB (MathWorks) script (Liaudanskaya et al., 2020). First, Otsu's thresholding was used to remove weak background fluorescence. Then, connected objects were identified using the bwlabel MATLAB function, and objects with eccentricity lower than 0.9 were removed, as they represented signals emanating from silk and cell bodies. The remaining voxels were grouped together into objects if neighboring edges or faces were in contact using the 3D bwlabel MATLAB function. The smallest ellipsoid was drawn around each object, and the major axis length of each individual ellipsoid was measured in voxel increments. The sum of all such voxels was calculated for each z-stack image to represent the volume occupied by neurites. The neurite density was presented as the percent of neurite voxel number to total voxel number per z stack.

Immunofluorescence analysis of 3D cultures

After chemical fixation of 3D cultures, the cells were permeabilized and blocked for 1 hr in blocking solution (4% (v/v) normal goat serum (Jackson Immuno Research #005-000-121) and 0.2% (v/v) Triton-X (MilliporeSigma #T8787) in PBS). Rabbit anti-GFAP primary antibody (1:2000, MilliporeSigma #G9269) and Alexa 488 goat-anti-rabbit secondary antibody (1:1000, ThermoFisher #A11034) were diluted in blocking buffer. Primary antibody incubation was done at 4°C overnight, followed by three 30-min PBS washes. Secondary antibody incubation was done in blocking solution at room temperature for 2 hrs, followed by DAPI staining (1:1000 in 0.2% Triton-X, Thermo Fisher #D1306) and three 30-min PBS washes. Confocal z stack images were acquired using a Leica SP8 confocal microscope with a 25X objective (Leica HC FLUOTAR L 25x/0.95 W VISIR) and with excitation lasers at 405 and 488 µm.

Gene expression analysis of 3D cultures

On 1, 14, 21 DIV, 3D culture samples were collected in 600 - 700 µL ice-cold Buffer RLT (Qiagen #79216) with 1% β-mercaptoethanol (MilliporeSigma #M3148) and stored in -80°C until RNA isolation. On the day of mRNA isolation, samples were thawed and homogenized, first by manually grinding into fine pieces with a homogenizer pestle (Fisher #12-141-364), followed by homogenization for 20 sec with a motorized tissue grinder (Fisher #12-1413-61), and then passed through a QIAshredder column (Qiagen #79656). RNA was isolated using the Qiagen RNeasy Mini Kit (Qiagen #79656) according to the manufacturer's protocol, with additional in-column removal of genomic DNA with DNase (Qiagen # 79254). The resulting RNA was eluted with 25-30 µL of water and the resulting concentrations measured using a NanoDrop Spectrophotometer (ThermoFisher). cDNA was synthesized using iScript gDNA Clear cDNA Synthesis Kit (Bio-Rad #1725035) according to the manufacturer's protocol.

Relative gene expressions were quantified using the Taqman quantitative real-time PCR (qRT-PCR) assay and analyzed with the QuantStudio 5 RT-PCR System (Thermo Fisher). Each qRT-PCR reaction contained

10 ng cDNA, 10 µL Taqman Gene Expression Master Mix (ThermoFisher #4369016), and 1 µL Taqman assay. See Table 2 for the list of Taqman assays. All expressions were referenced to housekeeping gene Rn18s and normalized to 1 DIV. ΔΔCt method was used to calculated relative expression levels.

DNA Quantification

Relative DNA amount was quantified using Quant-iT PicoGreen dsDNA Assay Kit (ThermoFisher # P7589). Cortical cell suspensions (1 and 2 x 10^6 cells) were centrifuged at 500 rpm for 5 min. Supernatant was removed, and cell pellets were lyzed with 700 µL Buffer RLT with 1% β-mercaptoethanol and vortex. 3D cultures were lyzed as described in the Gene expression analysis of 3D cultures section above. 5 µL samples or DNA standards were diluted with 95 µL Buffer RLT with 1% β-mercaptoethanol. Assays were conducted according to the manufacturer's protocol. Raw fluorescence values were used to estimate number of cells in the 3D cultures.

Ca^{++} imaging

A half-medium change was done 1 or 2 days prior to the day of imaging. Ca^{++} imaging was performed on AAV-hSyn1-GCaMP6f infected 3D cultures with a Nikon Eclipse Ti-2 inverted fluorescence microscope with a 4X objective (Nikon CFI Plan Fluor DL 4x na 0.13 wd 16.5mm Objective). During imaging, plates were kept at 37˚C and 5% CO_2 in a stage-top incubator (Bioscience Tools #TC-MWP). Medium was removed to keep the 3D cultures from floating during image acquisition, leaving approximately 500 µL of medium to support the culture during imaging. The 3D culture was centered in the field of view and all time-lapse images were acquired with a FITC filter and the following settings: 3x3 binning, 50-ms exposure, 200-ms intervals (i.e. 5 Hz), and 1-min duration. At 2 weeks (14 DIV) only spontaneous baseline Ca^{++} activities were recorded. At 3 weeks (20-22 DIV), a 1-minute baseline image analysis was first performed. Picrotoxin (50 µM, Abcam #ab120315) and bicuculline (10 µM, Abcam #ab120107) were then applied for 7 min to the sample, after which recording was repeated for another minute. NBQX (5 µM Tocris 1044; and AP5 (50 µM, Sigma A8054) were applied for 22 min before the second recording. Picrotoxin and bicuculline were first dissolved in DMSO to make 2000X stock solutions. A 5 µL of a 100X concentrated solution, diluted in Neuro Medium, of each of the drugs was added to the cultures. Equivalent concentration of DMSO (1:2000) was added to a separate set of 3D to control for the addition of DMSO in picrotoxin and bicuculline. The time-lapse images were converted to TIFF stacks in NIS-Elements software (Nikon).

Neuronal activity and global synchronization analysis of 3D neural networks

Region of interest (ROI) assignment

A mask in the shape of a honeycomb pattern of 37 hexagonal ROIs (side-to-side distance = 500 µm, center-to-center distance = 500 µm) was first designed on Adobe Illustrator to cover the circular projection of the 3D scaffold and converted to binary in Adobe Photoshop or NIS-Elements (Nikon, Micro Video Instruments, Inc). Each ROI was defined as a node for all of the following analyses.

Ca^{++} events detection, % active ROI, and Ca^{++} event frequency calculation

Ca^{++} event detection and event frequency calculation were conducted using an open source MATLAB-based software FluoroSNNAP (Patel et al., 2015). The time-lapse TIFF stack and ROI mask were loaded in FluoroSNNAP, and the Segmentation GUI was used to create a segmentation MATLAB. The *Single-Cell Ca^{++} Transient Kinetics* module was used for Ca^{++} event detection and to calculate total events for each individual ROI in a 3D tissue sample. The input parameters used for baseline fluorescence were F_0 = 10

sec of previous and 20th percentile. The input parameters for Ca^{++} event detection were template-based, threshold = 0.85, and minimum dF/F amplitude = 0.01. Descriptions of input parameters are detailed in (Patel et al., 2015). Samples with poor cell seeding efficiency (< 50% active ROI at baseline) were excluded.

% Active ROI and Ca^{++} event frequency of each 3D tissue was calculated as:

$$\%\ Active\ ROI = \% \frac{Number\ of\ ROIs\ containing\ at\ least\ one\ Ca^{++}event}{N} \quad \text{Eq. 1}$$

$$Ca^{++}event\ frequency_{Single\ ROI} = \frac{Number\ of\ events}{1\ min} \quad \text{Eq. 2}$$

$$Ca^{++}\ event\ frequeycy_{tissue} = \frac{1}{N}\sum Ca^{++}event\ frequency_{Single\ ROI}) \quad \text{Eq. 3}$$

where N is the total number of nodes, which is 37 in this study.

Global synchronization Index

Global synchronization index was calculated using FluoroSNNAP's *Synchronization* module with input parameters of method = Phase, #times to perform surrogate resampling = 20, minimum size of synchronization cluster = 3. The mathematical descriptions are detailed in (Patel et al., 2015). Briefly, this method separates the time-varying fluorescence signals into its amplitude and phase components and compares the similarity of timing of events (phase) of all the ROIs.

Functional connectivity and graph theory-based network analysis of 3D neural networks

Cross-correlation analysis

Cross-correlation analyses were done using FluoroSNNAP's *Estimate Functional Connectivity* module, with number of resampling = 100 and significance level = 0.5. The raw cross-correlation coefficient matrices of all node (ROI) pairs (i, j, whereas i≠j) were accessed in the output MATLAB file (located in the file 'processed analysis.mat/FC/C'), extracted, and saved as a numeric matrix MATLAB file. This file is then loaded into a single, user-friendly, MATLAB code, which is a compilation of the individual codes used to compute the graph theory-based network parameters.

Average edge weight calculation

Network analyses in our study were based on a weighted network (i.e. edges values, not binary). The cross-correlation coefficients between paired nodes i and j were used as edge weights in the graph. The average edge weight for each 3D culture sample was calculated by averaging all the edge weights.

Average clustering coefficient and path length

The local clustering coefficient for each node c_i in a weighted graph was computed as described by Onnela et al, using their published MATLAB script (Onnela et al., 2005). Briefly, clustering coefficient in a weighted graph reflects the intensity of triangle networks formed by triplets of nodes is calculated as follows:

$$c_i = \frac{1}{k_i(k_i-1)} \sum_{j,k} \frac{\sqrt[3]{w_{ij}w_{jk}w_{ik}}}{\max(w)}$$ Eq. 4

where k_i is the number edges connected to node *j* (36 in our case) and *w* is the edge weight. The average clustering coefficient for a network C is the average of all c_i:

$$C = \frac{1}{N} \sum c_i$$ Eq. 5

where N is the total number of nodes.

Average path length

Path length for the 3D culture network was computed as described by Muldoon et al., 2016 using their published MATLAB script (Muldoon et al., 2016). Briefly, the shortest distance *d* between node i to node j is inversely proportional to edge weight (w) and is defined as:

$$d_{ij} = \frac{1}{w_{ij}}$$ Eq 6.

The average path length (PL) for a network PL_N, with number of nodes N is calculated as:

$$PL_{i,j} = \frac{1}{N(N-1)} \sum_{i \neq j} d_{ij}$$ Eq 7.

Number of modules and modularity

Module assignment of nodes and modularity were computed as described in Newman, 2006 using their published MATLAB script (Newman, 2006). Briefly, modularity is the sum of edges falling into a module minus the sum of expected edges in an equivalent random network. Module assignment is based on maximizing modularity of the network.

Node degree and determination of hubs

To calculate the node degree for each node, the sum of edge weights incident to the node was calculated. The frequency distribution (%) of individual weight node degree in all samples under the same condition was calculated with bin size = 0.05 using GraphPad Prism.

$$Weighted\ node\ degree_i = \frac{1}{A} \sum_{i \neq j} w_{ij}$$ Eq. 8

To test if the frequency distribution of weighted node degree followed a normal distribution, a Kolmogorov-Smirnov normality test was performed.

Statistical analysis

Statistical tests were performed using GraphPad Prism. Statistical significance in changes in neurite density (Fig. 2C) and mRNA expression (Fig. 2D and 3A) were tested with ANOVA with post-hoc Tukey tests. For changes in neuronal activity (Fig. 4E, F) between different cultures at 2 and 3 weeks, unpaired t-tests were used. Differences in neuronal activity (Fig. 5B-D) and network properties (Fig. 6C-F) between baseline and post-treatments of each individual 3D tissue were determined with paired t-tests. A p-value of 0.05 was used for significance level.

Supplementary Figures

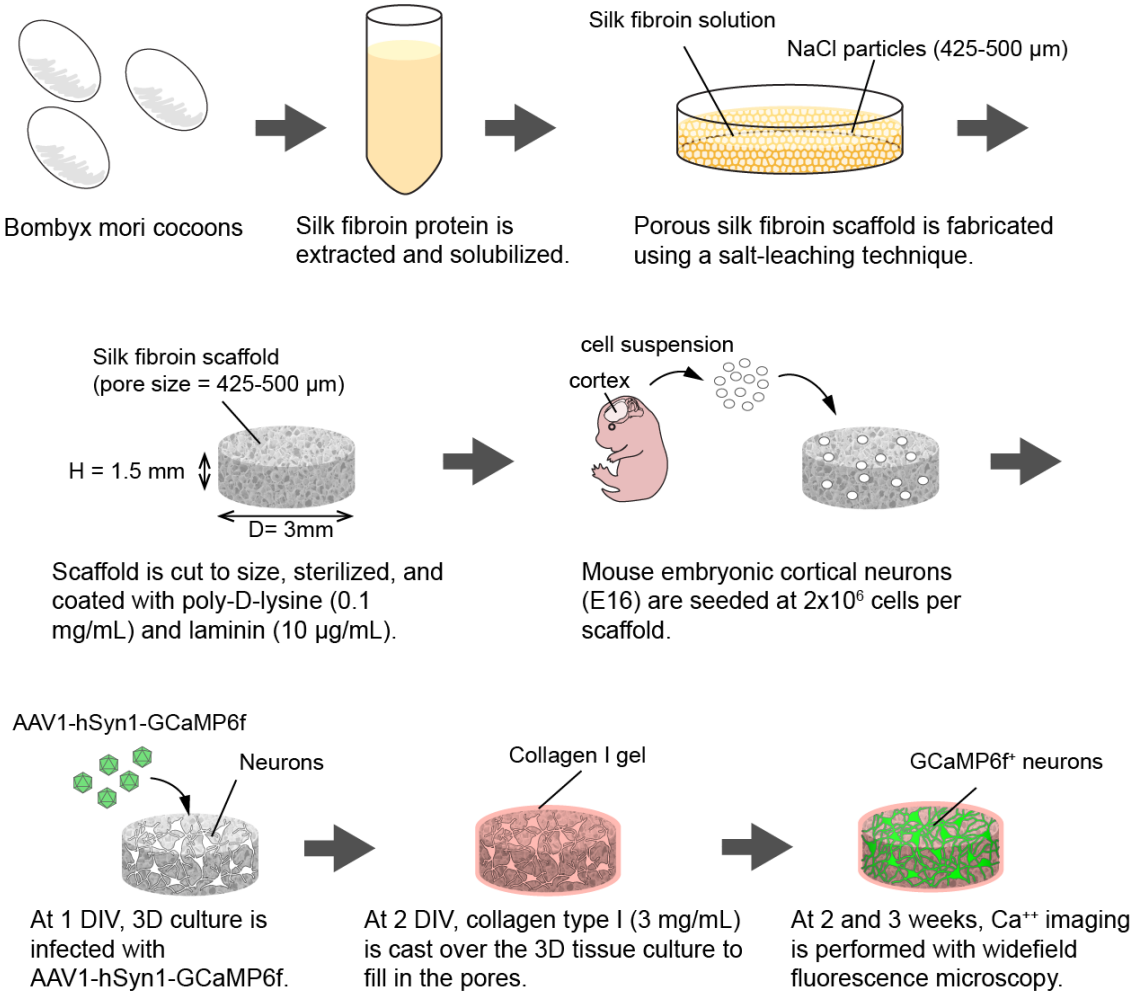

Figure S1. Schematic of the 3D *in vitro* cortical culture set up for cellular and network activity recording. Related to Figure 1.

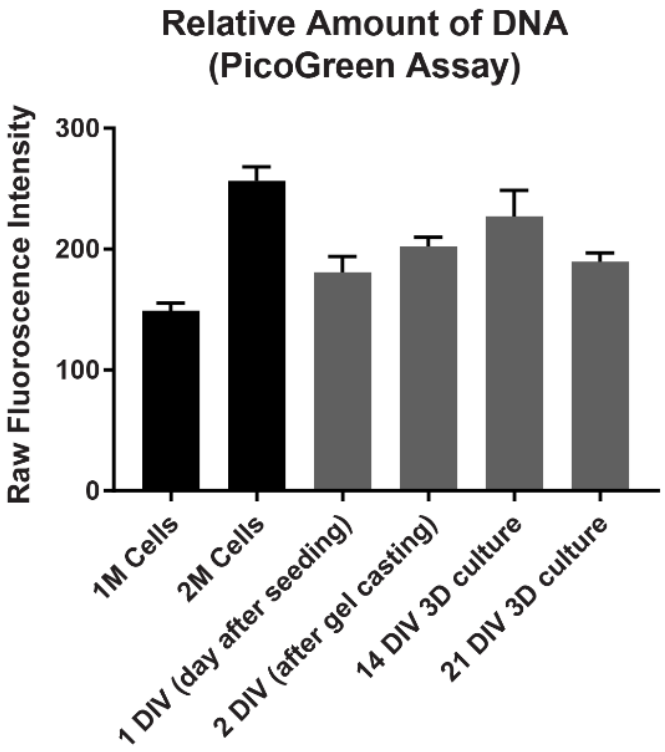

Figure S2. Relative cell numbers in 3D culture. DNA quantity in cortical cell pellets (1 and 2 million) and in 3D cultures were analyzed with PicoGreen DNA Quantification Kit. n = 3-5 samples. Related to Figure 1.

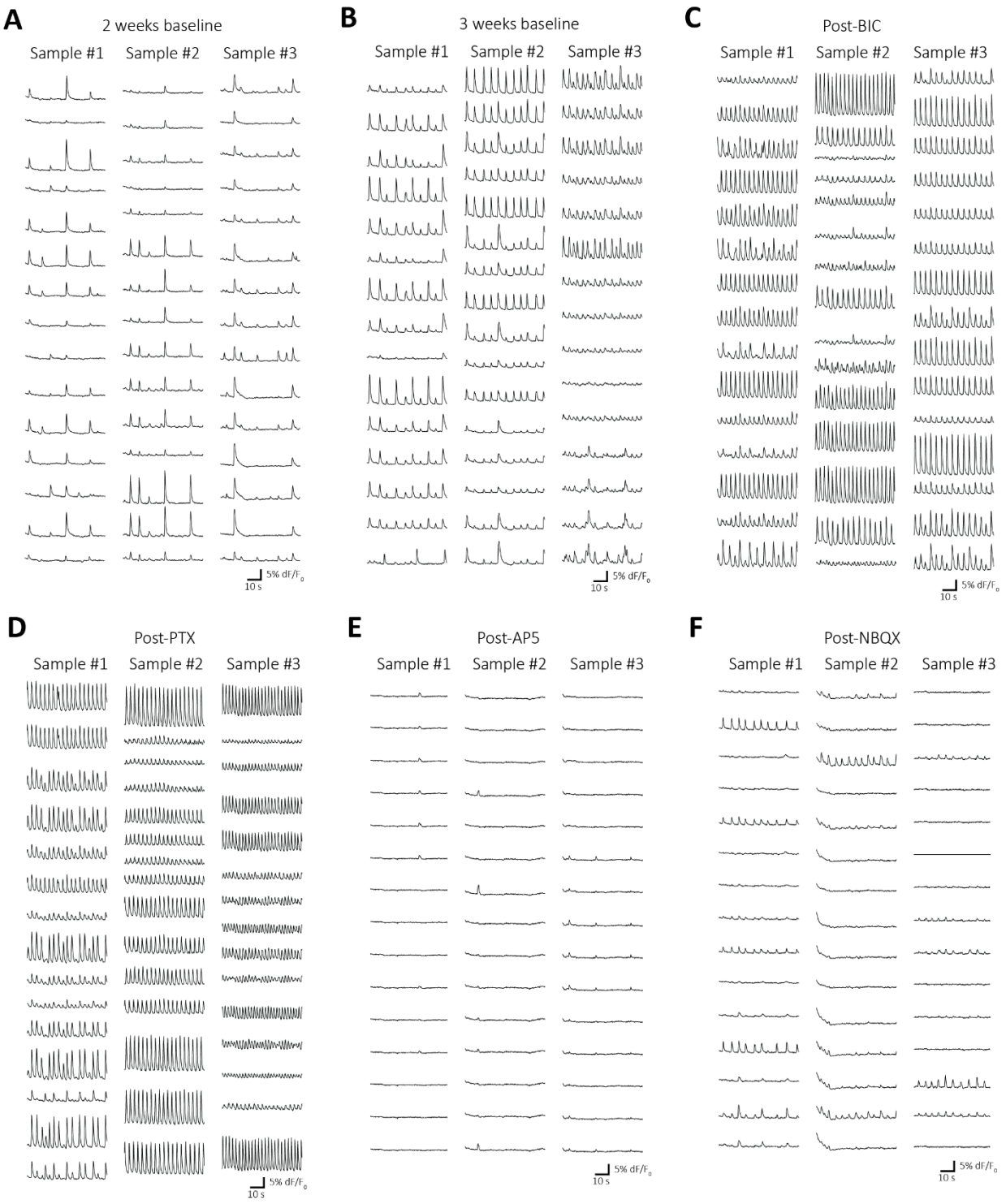

Figure S3. Example traces of Ca^{++} transients from three independent 3D *in vitro* biomimetic cortical cultures at (A) 2 weeks and (B) 3 week at baseline and post-drug treatments (3 wks only) of (C) bicuculline (BCC, 10 µM), (D) picrotoxin (PTX, 50 µM) (E) AP5 (50 µM), and (F) NBQX (5 µM). Each trace represents the average fluorescence intensity over time normalized to its basal fluorescence level (dF/F_0) from an individual hexagonal ROI (side-to-side distance 500 µm). Related to Figures 4-5.

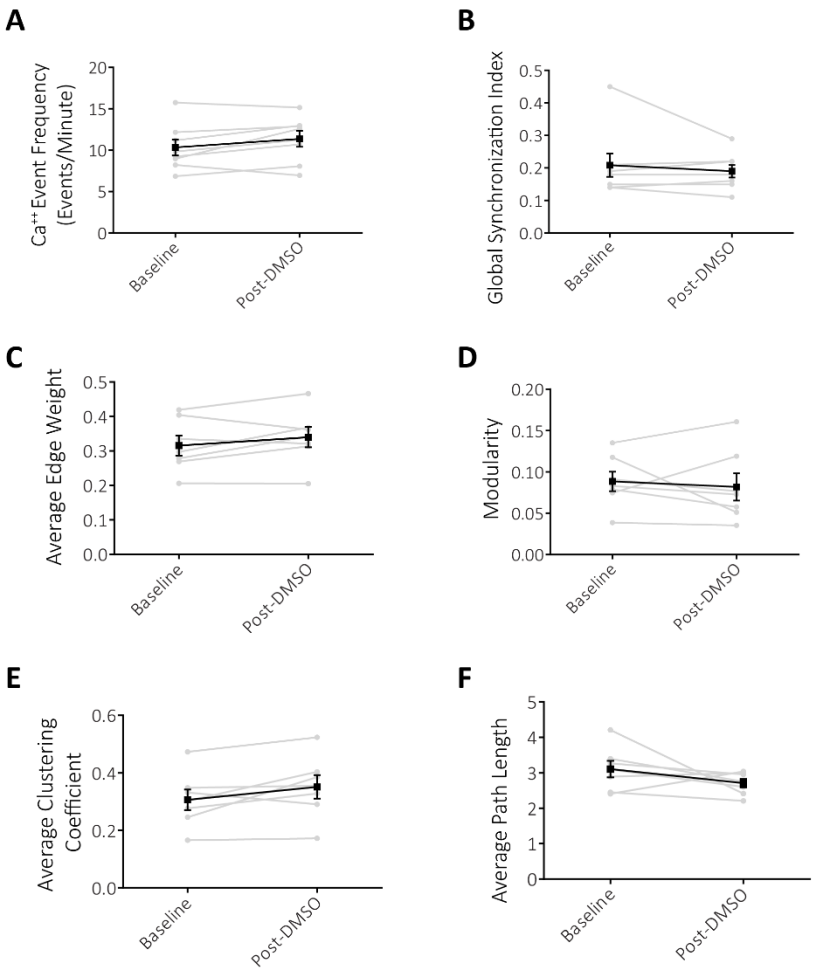

Figure S4. Control experiments with DMSO treatment, at the equivalent concentration (0.5%) as for BCC and PTX treatments, did not induce changes in (A) Ca^{++} event frequency, (B) global synchronization index, (C) average edge weight, (D) modularity, (E) average clustering coefficient, and (F) average path length. Grey data points and lines indicate baseline and post-treatment measurements of the same 3D tissue culture samples, and color lines show Mean ± SEM. n = 7 from two independent experiments. Related to Figure 5.

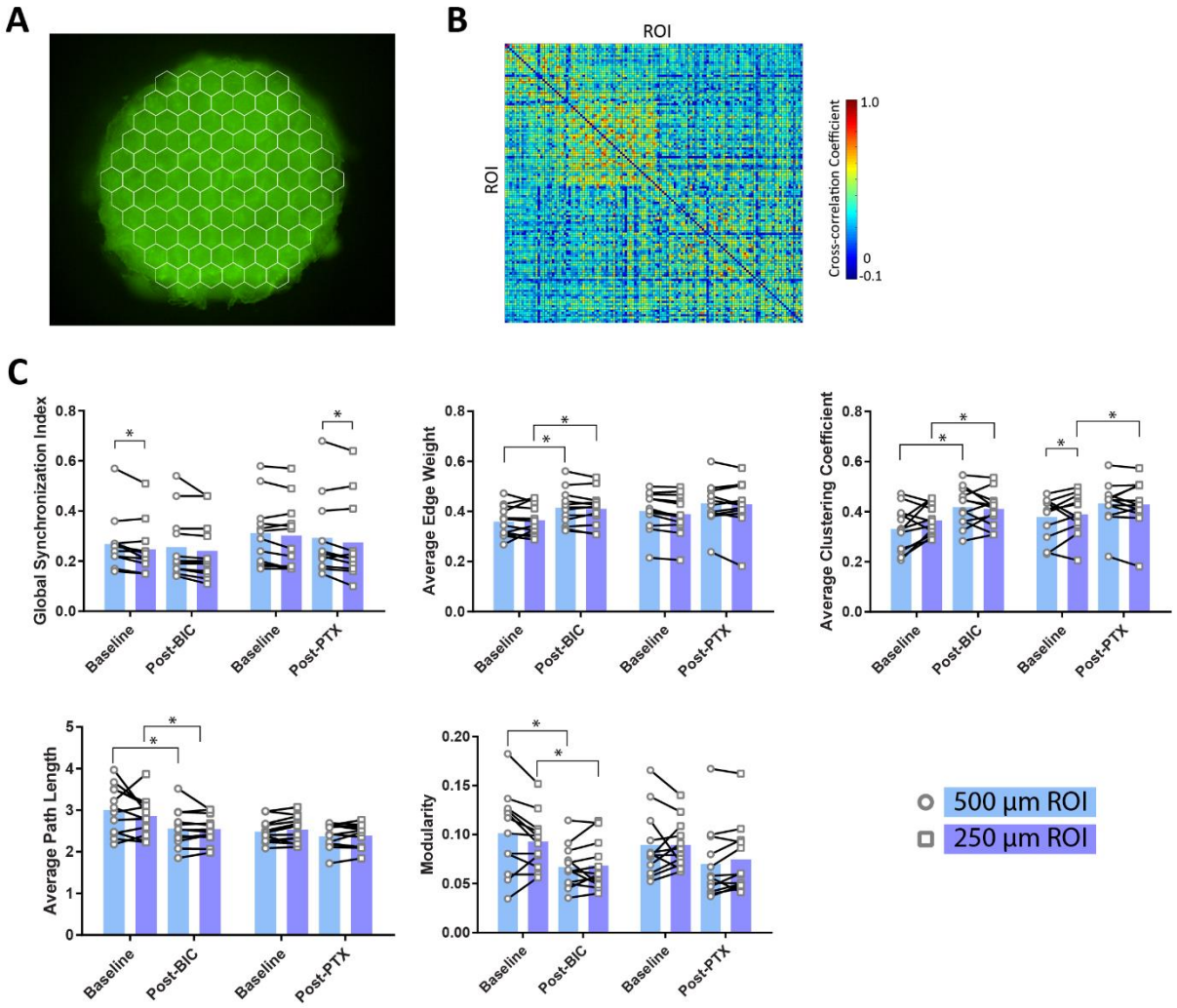

Figure S5. Network analysis with 500 µm vs 250 µm ROIs. (A) Time-lapse image stacks were applied with 127 hexagonal ROIs with side-to-side distance of 250 µm. (B) Representative cross-correlation matrix of neuronal activities in each ROI at baseline condition. (C) Network descriptors of global synchronization index, average edge weight, average clustering coefficient, average path length, and modularity, calculated based on using 500 µm or 250 µm ROI mask. Data are induvial values and Mean ± SD (n = 12 samples each group). Paired t-tests were used for statistical significance comparing the same condition with 500 µm or 250 µm ROI and for comparing baseline and post-treatment of the same sample with same ROI size. *p < 0.05. Related to Figure 6.

Drug		**Bicuculline**		**Picrotoxin**		**NBQX**		**AP5**	
Concentration		10 μM		50 μM		5 μM		50 μM	
Target and mechanism of action		Competitive $GABA_A$ receptor antagonist		Non-competitive $GABA_A$ and GABAρ receptors antagonist		Competitive AMPA receptor antagonist		Competitive NMDA receptor antagonist	
Sample Number		12		12		9		11	
Condition		Baseline	Post-Treatment	Baseline	Post-Treatment	Baseline	Post-Treatment	Baseline	Post-Treatment
% ROI	Min	94.59	100	89.18	100	94.59	16.22	89.19	0
	Median	100	100	100	100	98.65	48.65	100	32.43
	Max	100	100	100	100	100	100	100	100
Unpaired t-test		p = 0.3388		p = 0.3388		p = 0.0068		p < 0.0001	
Ca^{++} Event Frequency (events/min) (Mean ± SEM)		10.88 ± 1.10	15.41 ± 0.72	12.30 ± 1.10	17.80 ± 1.08	10.47 ± 1.05	2.68 ± 0.94	11.48 ± 1.61	0.35 ± 0.12
paired t-test		p = 0.0002		p = 0.0013		p < 0.0001		p < 0.0001	
Global Synchronization Index (Mean ± SEM)		0.269 ± 0.031	0.256 ± 0.037	0.312 ± 0.038	0.293 ± 0.045	0.268 ± 0.027	0.142 ± 0.035	n.a.	
paired t-test		p = 0.4105		p = 0.6981		p = 0.0273			
Average Edge Weight (Mean ± SEM)		0.360 ± 0.018	0.414 ± 0.021	0.402 ± 0.023	0.433 ± 0.025	0.394 ± 0.032	0.118 ± 0.051	n.a.	
paired t-test		p = 0.0134		p = 0.147		p = 0.0009			
Average Clustering Coefficient (Mean ± SEM)		0.331 ± 0.025	0.419 ± 0.023	0.380 ± 0.024	0.433 ± 0.025	0.358 ± 0.036	0.117 ± 0.043	n.a.	
paired t-test		p = 0.0057		p = 0.0711		p = 0.0005			
Average Path Length (Mean ± SEM)		3.01 ± 0.168	2.56 ± 0.13	2.49 ± 0.09	2.37 ± 0.08	n.a.		n.a.	
paired t-test		p = 0.0331		p = 0.2740					
n. of Modules (n. of samples)	with 3 modules	4	3	3	2	2	0	n.a.	
	with 2 modules	8	9	9	10	7	6		
	with 1 module	0	0	0	0	0	3		
Modularity (Mean ± SEM)		0.102 ± 0.012	0.067 ± 0.006	0.090 ± 0.010	0.070 ± 0.011	0.083 ± 0.018	0.083 ± 0.184 (N. Mod > 1)	n.a.	
paired t-test		p = 0.0173		p = 0.2043		p = 0.0202 (N. Module >1)			

Table S1. Results summary of neuronal activity measurements and functional network descriptors of the 3D *in vitro* biomimetic cultures at baseline and post-bicuculline, picrotoxin, NBQX, and AP5 treatments at 3 weeks. Related to Figures 4-6.

Gene	Encoded Protein	ThermoFisher Taqman Assay ID
Dcx	Doublecortin	Mm00438400_m1
Gabra1	Gamma-aminobutyric acid type A receptor alpha1 subunit	Mm00439046_m1
Gad2	Glutamate Decarboxylase 2	Mm00484623_m1
Gria1	Glutamate Ionotropic Receptor AMPA Type Subunit 1	Mm00433753_m1
Grin1	Glutamate Ionotropic Receptor NMDA Type Subunit 1	Mm00433790_m1
Pax6	Paired Box Protein Pax-6	Mm00443081_m1
Rn18s	18s Ribosomal RNA, 45s Ribosomal RNA	Mm03928990_g1
Shank3	SH3/ankyrin domain gene 3	Mm00498775_m1
Slc17a7	Vesicular glutamate transporter 1	Mm00812886_m1
Slc1a3	Excitatory amino acid transporter 1	Mm00600697_m1
Syn1	Synapsin I	Mm00449772_m1

Table S2. Taqman assays used in qRT-PCR in this study. Related to Figure 2.

SI References

Chwalek, K., Tang-Schomer, M.D., Omenetto, F.G., and Kaplan, D.L. (2015). In vitro bioengineered model of cortical brain tissue. Nat Protoc *10*, 1362-1373.

Liaudanskaya, V., Chung, J.Y., Mizzoni, C., Rouleau, N., Berk, A.N., Wu, L., Turner, J.A., Georgakoudi, I., Whalen, M.J., Nieland, T.J.F*., et al.* (2020). Modeling Controlled Cortical Impact Injury in 3D Brain-Like Tissue Cultures. Adv. Healthcare Mater. *9*, 2000122 doi.org/10.1002/adhm.202000122

Muldoon, S.F., Bridgeford, E.W., and Bassett, D.S. (2016). Small-World Propensity and Weighted Brain Networks. Sci Rep *6*, 22057.

Newman, M.E. (2006). Modularity and community structure in networks. Proc Natl Acad Sci U S A *103*, 8577-8582.

Onnela, J.P., Saramaki, J., Kertesz, J., and Kaski, K. (2005). Intensity and coherence of motifs in weighted complex networks. Phys Rev E Stat Nonlin Soft Matter Phys *71*, 065103.

Patel, T.P., Man, K., Firestein, B.L., and Meaney, D.F. (2015). Automated quantification of neuronal networks and single-cell calcium dynamics using calcium imaging. J Neurosci Methods *243*, 26-38.

Tang-Schomer, M.D., White, J.D., Tien, L.W., Schmitt, L.I., Valentin, T.M., Graziano, D.J., Hopkins, A.M., Omenetto, F.G., Haydon, P.G., and Kaplan, D.L. (2014). Bioengineered functional brain-like cortical tissue. Proc Natl Acad Sci U S A *111*, 13811-13816.